The Journal of Experimental Biology 200, 557–582 (1997)
Printed in Great Britain © The Company of Biologists Limited 1997
JEB0424

DRAGONFLY FLIGHT

II. VELOCITIES, ACCELERATIONS AND KINEMATICS OF FLAPPING FLIGHT

J. M. WAKELING* AND C. P. ELLINGTON
Department of Zoology, University of Cambridge, Downing Street, Cambridge CB2 3EJ, UK

Accepted 28 October 1996

Summary

The free flapping flight of the dragonfly *Sympetrum sanguineum* and the damselfly *Calopteryx splendens* was filmed in a large flight enclosure at 3000 frames s^{-1}. The wingtip kinematics are described for these flights. Despite the two species being similar in size, the damselfly flew with wingbeat frequencies half those of the dragonfly. The damselfly could perform a clap and fling, and the proximity to which the wings approached each other during this manoeuvre correlated with the total force produced during the wingstroke. The dragonfly beat its wings with a set inclination of the stroke planes with respect to the londitudinal body axis; the damselfly, in contrast, showed a greater variation in this angle. Both species aligned their stroke planes to be nearly normal to the direction of the resultant force, the thrust. In order to achieve this, the dragonfly body alignment correlated with the direction of thrust. However, the damselfly body alignment was independent of the thrust direction. Velocities and accelerations were greater for the dragonfly than for the damselfly. However, non-dimensional velocities and accelerations normalised by the wingbeat periods were greater for the damselfly.

Key words: dragonfly, damselfly, *Sympetrum sanguineum*, *Calopteryx splendens*, kinematics, velocity, acceleration.

Introduction

Dragonfly flight has fascinated scientists for most of this century. These insects are large, colourful and striking, and thus readily capture one's attention as they fly past. The dragonfly Order Odonata represents one of the oldest and most primitive forms of insect flight, with two pairs of wings which can beat independently. This primitive flight mode has also been a focus for attention, but it should by no means be considered simple: flight with two pairs of wings may require more complicated aerodynamic modelling than for the more derived insects with one functional pair of wings.

Considerations of dragonfly flight first appeared in the literature in 1921 when Hankin discussed the possible effects that air temperature and the sun have on the prevalence of gliding. High-speed cinematography for a range of dragonflies was first described by Magnan (1934), who took films of tethered dragonflies at 3200 frames s^{-1} and measured their stroke amplitudes and wingbeat frequencies. Magnan concluded that Zygoptera flew with greater stroke amplitudes than did Anisoptera. Chadwick (1940) also published high-speed kinematic data for a tethered dragonfly, and described its stroke amplitude and wingbeat frequency. In a study of the ventilation of flying insects, Weis-Fogh (1967) published some measurements for the wingbeat frequency and stroke amplitude of two tethered dragonflies.

In a study of the hovering flight of a range of insects, Weis-Fogh (1973) outlined some of the problems that may be experienced by flying dragonflies. Using a quasi-steady analysis, he assumed that the forces acting on an insect wing at each instant were the same as if that wing were in a steady flow with the same relative velocity; these forces were then averaged over the whole wingbeat cycle. Weis-Fogh (1973) showed that the mean lift forces required for flight are greater than quasi-steady values for a variety of insects, including the dragonfly. These insects must therefore rely on the extra lift generated by unsteady wing motion: i.e. wing rotations and accelerations. Renewed interest was thus sparked in the understanding of dragonfly flight to try to explain the high-lift mechanisms involved.

The free hovering flight of *Aeshna juncea* was filmed in the field by Norberg (1975). He described how this dragonfly hovered with a horizontal body and a steeply inclined stroke plane. This orientation required even greater lift, because weight support is only possible on the downstroke. This is in contrast to insects hovering with a 'normal' horizontal stroke plane, where lift on both the morphological up- and downstrokes can be used for weight support. Using a couple of alternative assumptions, Norberg (1975) confirmed that the quasi-steady mechanism is indeed insufficient to explain the lift required by flying dragonflies.

*Present address: Gatty Marine Laboratory, School of Biological and Medical Sciences, University of St Andrews, Fife KY16 8LB, UK (e-mail: jmw5@st-andrews.ac.uk).

The wingbeat kinematics of *Calopteryx splendens* were described by Rudolph (1976*a*,*b*), although they had previously been investigated by Magnan (1934). Rudolph noted that the wings of this damselfly can perform the 'clap and fling', a wing motion originally described by Weis-Fogh (1973) for the wasp *Encarsia formosa*. As the wings reach the dorsalmost position of their stroke, they clap together with the wing surfaces touching; they then fling apart, rotating about their trailing edges, as they separate on the downstroke. As the wings fling apart, a flow of air into the opening gap creates circulation about each wing. Weis-Fogh (1973) suggested that this mechanism may be a source of lift enhancement. An advantage of the fling-generated circulation is that it occurs before, and completely independently of, the translatory motion of the wing. The fling mechanism has been analysed theoretically (Lighthill, 1973; Edwards and Cheng, 1982; Wu and Hu-Chen, 1984), modelled numerically (Haussling, 1979) and verified experimentally (Bennett, 1977; Maxworthy, 1979; Spedding and Maxworthy, 1986), and it has been shown to produce higher transient circulations and lift forces than are possible from translatory motion alone.

The fling mechanism is not a discrete event, and there is a spectrum of insect wingbeat styles that differ in the dorsal position reached by the wings. Wings that only partially come together perform a partial fling, and those that do not quite touch perform a near fling (Ellington, 1984*c*). The separation between the wings when they fling apart may provide fine control over the circulation and thus the lift generated. This has been confirmed in model experiments by Sunada *et al.* (1993) and is seen in the locust (Cooter and Baker, 1977), where the hindwings perform a clap and fling during climbing but not during horizontal flight.

The ability to perform a clap and fling is a difference between the wingbeat kinematics of the damselflies and dragonflies. There is only one cited example of a dragonfly performing a clap and fling: Alexander (1984) studied 91 high-speed film sequences of dragonflies (mainly *Libellula luctuosa* and *Celithemis elisa*) in tethered flight and found evidence for this wing motion in only one sequence. In a study of the maximum lift produced by flying insects, Marden (1987) found that insects with clap-and-fling wing motions achieved on average 25 % more muscle mass-specific lift than did animals with other types of wingbeat. In particular, the damselfly muscle mass-specific lift was 44 % greater than that of dragonflies. The clap-and-fling mechanism is clearly a method for insects to generate enhanced lift from their wing strokes and is used by the damselfly.

Dragonflies, unable to use the clap and fling, must rely on other unsteady lift mechanisms. Ellington (1984*c*) suggests that an isolated rotation of the wings, coupled with flexion of the wing, may generate additional lift in a similar way to the clap and fling. This combined motion causes the wing to rotate about its trailing edge, which should produce a leading-edge vortex of the correct sense for lift on subsequent translation. Verification of this flex mechanism has been hampered by the methods available for determining wing angles during rotation. Angle of rotation estimates for dragonflies are particularly prone to error at supination and pronation; during stroke reversal, the camber, which is generated by aerodynamic force on the wings (Ennos, 1988; Wootton, 1991), is also reversed. Thus, the wings change from being cambered in one direction, through being flat, to being cambered in the other direction, with a resultant change in wing chord. Angles of rotation based on measurements of the wing chord from a single view will thus be prone to errors due to fluctuations in the chord; these errors would be up to 20 ° for dragonflies. To overcome this problem, at least two views of the wing are required so that estimations are not based on chord length alone. Nevertheless, there is some evidence to support the flex idea: wing rotation has been visually estimated for Diptera (Ennos, 1989) showing rotational coefficients within the range required by the flex mechanism, a sharp lift pulse has been recorded when the wing of *Drosophila melanogaster* is rotated at supination (Zanker and Götz, 1990), and Dickinson (1994) provides evidence that rotation of a wing about its trailing edge can create vorticity that enhances lift during the subsequent stroke.

It is possible that high lift forces are generated during the isolated rotation and flexion of dragonfly wings. Also, precise control of the lift generated by the wingstroke may be achieved by small changes in the timing of the wing rotations at supination and pronation. If so, there may be little correlation between the wingbeat frequency, the stroke amplitude and the translatory angle of attack with the velocity and overall aerodynamic force generated during flight. Indeed, the free-flight kinematic studies of Azuma and co-workers (Azuma *et al.* 1985; Azuma and Watanabe, 1988; Azuma, 1992) found little correlation between velocity and angle of attack, stroke amplitude or wingbeat frequency. The only systematic change that they found was that the wingstroke plane tilted forwards at higher velocities to be more nearly normal to the direction of the velocity.

The most wide-ranging study of the free-flight kinematics of dragonflies has been undertaken by Rüppell (1985, 1989; Rüppell and Hilfert, 1993): angle of attack, stroke amplitude, wingbeat frequency, velocity and stroke plane angle are given for over 20 species covering the three sub-Orders Anisoptera, Zygoptera and the relict sub-Order Anisozygoptera. Damselflies are characterised by lower wingbeat frequencies, higher stroke amplitudes and lower velocities and accelerations than dragonflies. No individual wingbeat has been fully analysed for all its kinematic parameters, however, and so these data have not been used to determine how the individual parameters affect the flight of each dragonfly or damselfly. The lower wingbeat frequencies and higher stroke amplitudes of damselflies have also been described by Newman (1982).

One further way in which the wingbeat kinematics may affect aerodynamic performance is that the phase relationship between the fore- and hindwings may change the flow interactions between the wing pairs. Somps and Luttges (1985) measured the forces generated by a tethered dragonfly and recorded a single large lift peak for each cycle. Flow interactions between the fore- and hindwings produced this

single lift peak rather than the double peaks expected from the sum of the forces from two independent wing pairs. Flow-visualisation studies on a flapping model dragonfly showed that the fore- and hindwings generate the same vortical structures as an isolated wing except over a critical range of reduced flapping frequencies, pitching rates and phase relationships, where the vortices become more cohesive and even fuse, with a resultant lift enhancement (Saharon and Luttges, 1988; Luttges, 1989). Changing the kinematic parameters can alter the flow interactions between the wings, resulting in a change of aerodynamic force that could not be predicted solely from the flow around the individual wings. Luttges (1989) noted that the phase relationship between the wings affects the relative proportions of the horizontal and vertical components of the net aerodynamic force.

Dragonflies typically fly with their wings beating out of phase, or counterstroking. It has been suggested that beating their wings in phase, or parallel stroking, may produce higher aerodynamic forces (Alexander, 1984, 1986; Rüppell, 1989) and so may be used for high-lift situations such as rapid accelerations or tandem flying with a mate. In a theoretical study on the effects of the phasing relationship for a dragonfly wingbeat, Lan (1979) plotted the efficiency η and mean thrust coefficient $\bar{C}_T$ as functions of the phase lag of the forewings. On average, the predicted optimum phase lag was 90° for maximum energy extraction by the hindwings from the wake of the forewings; for maximum $\bar{C}_T$, the lag was 45°. Hence, as dragonflies increase the degree to which they beat their wings in parallel, the wings will generate more thrust at the expense of a lower efficiency.

In the present study, the free flights of *Sympetrum sanguineum* and *Calopteryx splendens* were filmed using a high-speed cine camera. These species are members of the sub-Orders Anisoptera and Zygoptera; they were chosen as they are individuals of approximately the same mass and wing area. For steady flight, the mean lift required by both species will be similar, but it may be generated by different kinematic mechanisms. However, the flight of *Calopteryx splendens* may not be representative of that of the Zygoptera as a whole. Calopterygidae have disproportionately large wing areas when compared with other Zygoptera (Grabow and Rüppell, 1995), leading to lower wing loadings. The smaller Zygoptera generally fly with their fore- and hindwings counterstroking with a near half-cycle phase shift (Rüppell, 1989). In contrast, the Calopterygidae can fly with very little phase shift between the wing pairs (Rüppell, 1985). Nonetheless, the Zygoptera, including *C. splendens*, are characterised by lower wingbeat frequencies and larger stroke amplitudes than the Anisoptera (Rüppell, 1989). Flights from the present study were unrestrained by either tethers or wind-tunnels, and so the insects were free to vary the velocity and acceleration at which they flew. However, the escape nature of the flights resulted in the directions of the velocity and acceleration being roughly correlated. Velocities and accelerations were derived from positional data on the films, and the total aerodynamic force was estimated. The flights were then used to compare the different wingbeat modes between the dragonflies and the damselflies, and also to determine whether any of the kinematic parameters could be correlated with the velocity or aerodynamic force.

Materials and methods

Dragonflies of the species *Sympetrum sanguineum* (Müller) and *Calopteryx splendens* (Harris) were caught at Quy Fen and Grantchester Meadows, Cambridge, respectively, during the period 3–30 July 1993. Upon capture, each individual was placed in a plastic box, which was stored in the dark inside an ice cooler. Once the dragonflies had cooled down, they ceased to struggle within their boxes. The dragonflies were transferred to a refrigerator in Cambridge and filmed within 24 h of capture. Before filming, the dragonflies in their boxes were left to warm up to ambient temperature for at least 10 min. The mean thermal time constants for *S. sanguineum* and *C. splendens* (=1/Newtonian cooling constant, values from Wakeling and Ellington, 1997*b*) were 143 s and 100 s, respectively, and so they would passively warm up to at least 98 % of the ambient temperature within 10 min. However, the dragonflies were active during this period and would heat up even faster, perhaps to temperatures above ambient. Flights were filmed in the specially adapted greenhouse described in Wakeling and Ellington (1997*a*). Flight behaviour resembled that seen in the field: both species commonly flew the length of the pond a couple of times before perching on the glass walls, the green netting or the vegetation around the pond.

The free flights of the dragonflies were filmed using a John Hadland P.I. Hyspeed cine camera. Ilford Pan F 16 mm black-and-white film was shot at 3000 frames s^{-1}; timing lights within the camera strobed at 1000 Hz to give a time reference on the films. A Cinor 50 mm fixed focal length lens was used at an aperture of *f*/11. The films were developed in a John Hadland P.I. 16/35B R2 negative film processor set to 30 °C and the slowest speed to enhance contrast. A 300 W halogen lamp was used to backlight the dragonflies to provide a silhouette image. The light was partially diffused through a frosted glass plate and was then focused through a Fresnel screen into the cine camera. This arrangement minimised the light intensity needed for filming and thus reduced the heat dissipated from the lamp. The Fresnel screen measured 0.2 m×0.3 m and was placed on the opposite side of the pond 2.2 m away from the cine camera. Dragonflies were released 1.8 m from the camera. Approximately 0.5 s after starting the camera, the top of the box was removed; this corresponds to the time taken for the film to accelerate up to speed. Characteristic flights for both species involved flying steeply out of the box and then taking a shallower course along the pond. Dragonflies flying out of the box necessarily entered the filming area, and this was recorded on 36 of the 95 sequences filmed. Ten *S. sanguineum* and four *C. splendens* individuals were filmed with no more than 10 sequences for each individual.

The dragonflies were filmed approximately 60 wing lengths away from the camera, and the frame covered a horizontal

distance of eight wing lengths. Analysis of the projection errors for this filming geometry (Ellington, 1984*b*) shows that the reconstructed angles will be less than 1 ° in error over the entire filming area and that the assumed horizontal plane will deviate by less than 1.6 ° from the true horizontal. Perspective errors can thus be ignored during the kinematic analysis.

Dragonflies were weighed before and after each filming session, and the mean was assumed to be the mass during the flight sequences. Dragonflies were killed with ethyl acetate immediately after filming. Measurements of wing and body morphology were made within 6 h of filming using methods described elsewhere (Wakeling, 1997).

Films were analysed using a Vanguard Instrument Corporation model M-16C 16 mm projection head as described by Ellington (1984*b*). Analogue output from the digitising device was read by a National Instruments MIO16L-9 12-bit analogue-to-digital converter in a Macintosh Quadra 650 computer. The coordinates of any point on the screen were accurate to 0.1 mm, or 0.2 % of the maximum projected wing length. This corresponds to a single bit from the analogue-to-digital converter. The accuracy of digitised sequences is thus limited by the image quality and the clarity of the wing outlines rather than by any inherent inaccuracies in the digitiser. The computerised three-dimensional reconstruction of the wing kinematics, as described by Ellington (1984*b*), had previously been coded by A. P. Willmott; this routine was modified to use a time-varying value for the maximum projected wing lengths as explained below. All other custom software was specifically written for this dragonfly study, mainly in LabView and Mathematica for Macintosh computers.

Velocities and accelerations

The films of the flying dragonflies consist of two-dimensional images taken from a single viewing direction. These images were digitised in a *y*,*z* coordinate system in which both the *y* and *z* axes are parallel to the film plane, with the *y* axis horizontal and the *z* axis vertical. All the information required to reconstruct the three-dimensional flight path must be taken from these images. The velocity of the dragonfly away from the camera is calculated along a horizontal *x* axis, which is perpendicular to both the *y* and *z* axes.

This study only investigated flights in which the acceleration during each sequence is linear and constant. Each film was initially tested for this condition as follows. The near forewing base position was digitised from every tenth frame, and the *y* and *z* coordinates were plotted against time. Least-squares linear, quadratic and cubic regression lines were fitted to these data. For flight at a constant velocity, the linear fit will be no worse than the quadratic or cubic fit; and for flight at a constant acceleration, the quadratic fit will be no worse than the cubic fit. The quality of each fitted regression line is judged by the root mean square (RMS) residual values, giving the variation of the data from that fitted line. Where the quadratic fit showed substantially larger RMS residual values than the cubic fit, the flight sequence was not consistent with a constant acceleration; in such a case, if a shorter section of that flight appeared to be at a constant acceleration, then that section was isolated and retested. Flight sequences were only considered for further analysis if they showed constant acceleration for several wingbeats. It is assumed that, if acceleration is constant along the *y* and *z* axes, then it will also be constant along the *x* axis. By definition, linear acceleration cannot have any rotatory component. Hence, the flight sequences considered here have negligible angular acceleration and this component is thus ignored.

Movement along the *x* axis was determined from changes in the image size. The distance *S* of an object from the optical centre of the camera lens can be calculated using simple lens theory:

$$S = f\left(1 + \frac{1}{M}\right), \quad (1)$$

where *f* is the focal length and *M* is the magnification (=image length/object length). The beating wings were used to act as a reference length for the dragonfly. During each wingbeat, the wings continually change orientation with respect to the film plane. In some cases, the wings pass through a position where they are parallel to the film plane; this gives the maximum projected wing length for that particular distance of the wing from the camera. The projected wing lengths are calculated from the digitised wingtip and wingbase positions from the *y*,*z* film coordinate system as:

$$\text{projected wing length} = \sqrt{(y_{\text{tip}} - y_{\text{base}})^2 + (z_{\text{tip}} - z_{\text{base}})^2}\,. \quad (2)$$

The true maximum projected wing length occurs twice for each each wingbeat. However, if the beating wing never passes parallel to the film plane, the projected length still reaches a maximum but there is only a single maximum per wingbeat. These two cases are distinguished in Fig. 1.

Whenever a dragonfly flight sequence generates a true maximum projected wing length for either the forewings or the hindwings, the distance from the wings to the optical centre of the lens can be calculated, giving the additional positional information along the *x* axis required for velocity and acceleration estimates.

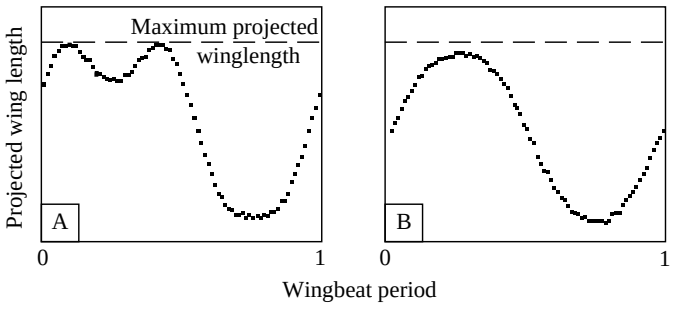

Fig. 1. Relationship between projected wing length and the wingbeat cycle for a recorded image of a beating wing. Projected wing lengths reach a true maximum where the wing passes through a position parallel to the film plane in A, but not in B. See Materials and methods for further details.

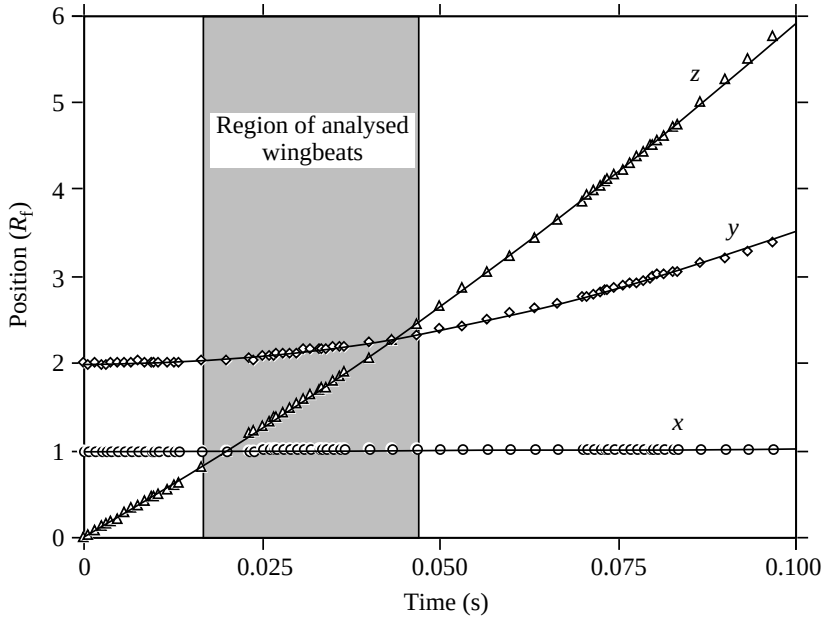

Fig. 2. Forewing wingbase positions for flight SSan6.1 of *Sympetrum sanguineum*. Positions are scaled relative to forewing length R_f. Data are shown for the range with constant acceleration where quadratic regressions are no worse than cubic equations. Least-squares quadratic regressions are shown with the data. The shaded region is the period from which the analysed wingbeat SSan6.1 is taken (see Fig. 4).

The film sequences which showed flight at a constant acceleration were redigitised, this time for the base and tip positions of the near wings in each frame; the projected wing lengths were then calculated for each frame. Where maximum projected wing lengths occurred, the non-dimensional distance in wing lengths, $\hat{S}$, from the camera was calculated:

$$\hat{S} = \frac{f}{R_f}\left(1 + \frac{1}{M}\right), \tag{3}$$

where R_f is the forewing length. Maximum projected wing lengths can occur for both the fore- and hindwings, and so the maximum hindwing lengths were normalised to the forewing length, and a pooled data set was used containing the maximum values from both wing pairs. Values for $\hat{S}$ for the frames in which there was no maximum projected wing length were taken as linear interpolations of the distances at which there was a maximum. These interpolated values will only be an estimate of the distance of the dragonfly from the camera, however, as the dragonflies accelerated and decelerated slightly within each wingbeat. Finally, a quadratic function was fitted to the non-dimensional x position from the camera against time. This least-squares quadratic fit follows the assumption that the flight occurred at constant acceleration. The function describing the x position was differentiated to obtain the non-dimensional x velocity and acceleration. Sample positional data are shown in Fig. 2. The maximum projected wing lengths were then also described by a least-squares quadratic fit. However, a cubic spline fit proved more useful for the kinematic reconstruction and is discussed more fully below.

The motion of the dragonfly along the y axis was calculated as a non-dimensional velocity in wing lengths s^{-1}, relative to the estimated maximum projected wing length for each frame. The mean y velocity during the wingbeat was the mean value from a linear least-squares regression of the non-dimensional y velocity against time, and the gradient of this line gave the non-dimensional y acceleration. Displacements in the z axis were treated in the same way as those in the y axis.

Velocity V and acceleration A were calculated from their x, y and z components using trigonometry. Non-dimensional velocity $\hat{V}$ is the velocity in wing lengths per wingbeat:

$$\hat{V} = \frac{V}{R_f n}, \tag{4}$$

where R is the forewing length and n is the mean wingbeat frequency. Non-dimensional acceleration $\hat{A}$ is the acceleration in wing lengths per wingbeat per wingbeat:

$$\hat{A} = \frac{A}{R_f n^2}. \tag{5}$$

The inclinations of the velocity and acceleration relative to the horizontal axis are given by ξ_V and ξ_A, respectively.

The total aerodynamic force generated by the dragonfly during a wingbeat must overcome its weight, acceleration and parasite drag D_{par}. The thrust T is the vector sum of these three forces and is discussed in greater detail in Wakeling and Ellington (1997*b*). In the present study, the thrust T is the total aerodynamic force, as in the helicopter literature; it is *not* the horizontal component of the aerodynamic force. Non-dimensional thrust $\hat{T}$ is thrust per body weight:

$$\hat{T} = \frac{T}{m\boldsymbol{g}}, \tag{6}$$

where m is mass and $\boldsymbol{g}$ is the acceleration due to gravity.

Values for R_f and m are given in Table 1; full morphological data for these insects are given in Wakeling and Ellington (1997*b*).

Table 1. *Morphological parameters used for the kinematic analysis*

Identity	m (mg)	R_f (mm)
SSan2	121.9	27.85
SSan5	133.0	27.23
SSan6	111.5	26.38
SSan9	139.3	29.44
CS1	91.0	30.43
CS2	93.6	29.44
CS3	123.6	30.42
CS4	119.1	29.68

Further parameters for these insects can be found in Wakeling and Ellington (1997*b*).

SSan, *Sympetrum sanguineum*; CS, *Calopteryx splendens*; m, mass; R_f, forewing length.

Kinematic reconstruction

The wingtip and body kinematics were reconstructed according to the protocol described in Ellington (1984*b*). This method takes the two-dimensional coordinates of the wings and body and transforms them through a series of coordinate systems as outlined below. The kinematic reconstruction assumes that the left and right wings beat symmetrically about the body, and so is able to use positional information from the far wings to calculate the body orientation relative to the camera. This assumption is most robust for straight flight and fully banked turns.

The kinematic analysis treats a single pair of wings, and so each wing pair from the dragonfly was analysed separately. For clarity, the methods outlined here describe analysis of the forewing only, but the method for the hindwing was identical. The following eight points around the dragonfly outline were digitised in the y,z system for each frame (Fig. 3): the most anterior and most posterior positions on the longitudinal body axis (head and anus), the base and tip positions for the 'near' fore- and hindwings (those where the base was visible throughout the stroke), and the tip positions for the 'far' fore- and hindwings. The origin of the y,z axes was taken to be the near forewing base (see Fig. 3). Discrete jumps in the wingtip position sometimes occurred between frames owing to light shining differently through the wing corrugations as the wings rotated with respect to the light source; this was most noticeable at supination and pronation.

The original analysis (Ellington, 1984*b*) used the maximum projected wing length for the wingbeat as a reference length with which to normalise the calculations. This is only suitable, however, when the maximum projected wing length and hence the distance from the camera does not change between wingbeats: i.e. for insects which are hovering, tethered or flying at a fixed position in a wind-tunnel. In the present study, the dragonflies were free-flying and frequently changed their distance from the camera. The maximum projected wing length increases by 4 % during a typical dragonfly wingbeat starting 60 wing lengths away from the camera and moving towards the camera at $\hat{V}$=2.4; it is thus important to incorporate a time-varying value for the maximum projected wing length. Within a wingbeat, the dragonfly's body will accelerate and decelerate, although the precise function of this motion is not known. Initially, the maximum projected wing length was estimated by a least-squares quadratic fit to the measured values. However, frames where projected wing lengths were greater than the predicted maximum led to a breakdown in the analysis. A cubic spline function was used instead to predict the maximum projected wing length for each frame, and this length was never smaller than the individual projected lengths. The cubic spline produced a smooth change in lengths between frames and was probably as good as any method for estimating the actual value.

An inherent problem in this analysis is that the reconstructed

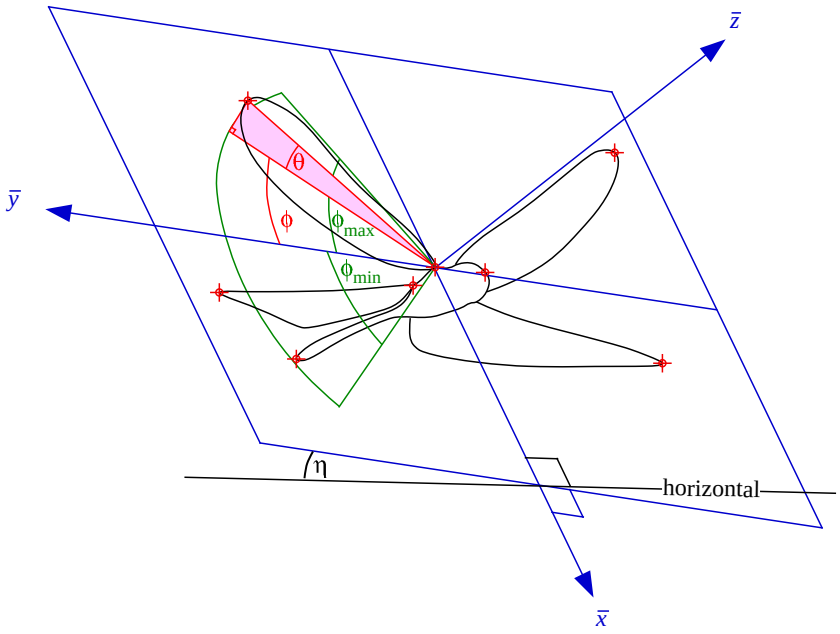

Fig. 3. Coordinate system for the wingtip kinematic analysis. Red crosses indicate the digitised positions. The $\bar{y}$ axis is parallel to the line joining the wingtips and lies in the stroke plane, and the $\bar{x}$ axis also lies in the stroke plane and is perpendicular to $\bar{y}$. The origin of the coordinate system passes through the near wingbase. Methods for creating this coordinate system can be found in Ellington (1984*b*). Roll η is the angle between the $\bar{y}$ axis and the horizontal. The wingtip position is described by the spherical coordinates (θ,ϕ) based around the stroke plane.

angles are sensitive to small measurement errors when the wing is close to maximum projection (Ellington, 1984*b*). This effect is sharply peaked, with errors dropping to ±3° for positions 10° on either side of the object plane. Significant errors can also occur around maximum projection if the value used for the maximum projected wing length is itself subject to digitising error. With the very high sampling rate per wingbeat used in this study, it is likely that values very close to the maximum projected wing length were measured several times. The maximum projected wing length may thus be a biased overestimate due to digitising error at both the wingbase and the wingtip. This is revealed by a characteristic discontinuity in the reconstructed angles around the position of maximum projection. In such cases, the value for the maximum projected wing length was decreased by up to 1% to remove the local discontinuity.

The time-varying maximum projected wing length was then used in Ellington's (1984*b*) protocol for wingtip kinematics. Yaw ψ is the horizontal component of the angle between the longitudinal body axis and each motion vector. Yaw was calculated with respect to both velocity, ψ_V, and acceleration, ψ_A. Roll of each wing pair η, body angle χ and stroke plane angle β are all calculated relative to the horizontal. The wingtip positions are described by spherical coordinates (ϕ,θ) (Fig. 3). The positional angle of the wing ϕ within the stroke plane takes positive values when the wing is dorsal, and negative values when it is when ventral. The angle of elevation θ of the wing from the stroke plane is positive when the wing lies above the stroke plane. The stroke plane angle β is calculated with the implicit assumption that no pitching occurs during the wingstroke. A mean body angle $\overline{\chi}$ is similarly taken to be the mean value for χ during the stroke.

Wingbeat frequency

Wingbeat frequency *n* was estimated directly from the films. A characteristic wing position was traced at either supination or pronation when a chord near the wingtip was vertical. The wingbeat period was the time until the wing returned to the same position after one wingbeat, with the tracing superimposed on the new wing image; time was measured relative to the timing markers on the film. Supination and pronation are rapid events with the wing quickly rotating through a large angle in a few frames, and so this method is accurate to within a single frame per wingbeat: typically 1.3% for *S. sanguineum* and 0.7% for *C. splendens*.

Fourier series analysis of the wingtip kinematics

Fourier series were fitted to describe ϕ and θ with time. Up to six terms were used to assess the importance of higher harmonics within the wingbeat. The standard error (S.E.M.) of each Fourier series was calculated so that the quality of the fits could be compared. The Fourier series applied to the data were:

$$\phi,\theta = \frac{a}{2} + \sum c_i \cos(it + o_i) , \quad (7)$$

with the standard errors:

$$\text{S.E.M.}_i = \sqrt{\frac{1}{N-(2i+1)} \sum (\text{observed} - \text{predicted})^2} , \quad (8)$$

where a, c_i and o_i are the Fourier coefficients, i is the harmonic number, t is time, and N is the number of data points within the wingbeat.

The films were recorded at very high sample rates per wingbeat, and so there are many data points around the maxima and minima of the ϕ curve. Each point is subject to digitising and analysis error, and so it is likely that the values for ϕ_{max} will be overestimated and those for ϕ_{min} underestimated. The Fourier series, however, smoothes through these regions and more accurately estimates ϕ_{max} and ϕ_{min}. The Fourier series using four harmonics predicts values for ϕ_{max} to be 1.9° smaller and ϕ_{min} to be 2.4° greater than the unsmoothed estimates. These discrepancies are consistent with the errors introduced during digitising and analysis, and so the maximum and minimum positional angles, ϕ_{max} and ϕ_{min}, were calculated from reconstructed wingbeats using four harmonics in the Fourier series for ϕ. The mean positional angle within the stroke plane, $\bar{\phi}$, is thus given by:

$$\bar{\phi} = \frac{\phi_{max} - \phi_{min}}{2} , \quad (9)$$

and the total stroke amplitude is Φ ($=\phi_{max}-\phi_{min}$). The ratio of the downstroke to upstroke duration, d/u, is given by the ratio of the period from ϕ_{max} to ϕ_{min} to the period from ϕ_{min} to ϕ_{max}.

Results

Flight sequences had to pass two criteria before they were fully analysed. The sequences had to show at least one complete wingbeat in which all four wingtips were visible and in which the near wings passed through the film plane, yielding true maximum projected wing lengths. Second, each sequence had to be for a flight in which the mean acceleration of the body was constant. From a total of 95 films, 36 had flight sequences on them, with seven for *S. sanguineum* and nine for *C. splendens* passing the criteria for analysis. These data were from four *S. sanguineum* and four *C. splendens* individuals. Examples of these sequences are presented in Figs 4 and 5. Examples of the time series for ϕ and θ are shown in Fig. 6 for both *S. sanguineum* and *C. splendens*. Reconstructions of the wingbeats are shown in Fig. 7 for *S. sanguineum* and Fig. 8 for *C. splendens*. Sequences are identified by a prefix SSan or CS, referring to *S. sanguineum* and *C. splendens*, respectively, followed by a number, referring to the individual's identification number, and finally a decimal point and a number categorising that flight.

The kinematic diagrams

The upper drawings in Figs 7 and 8 show the dragonfly body with its velocity and acceleration vectors. For clarity, each drawing has been reconstructed in perspective. Around the dragonfly body is a circle with radius equal to the forewing

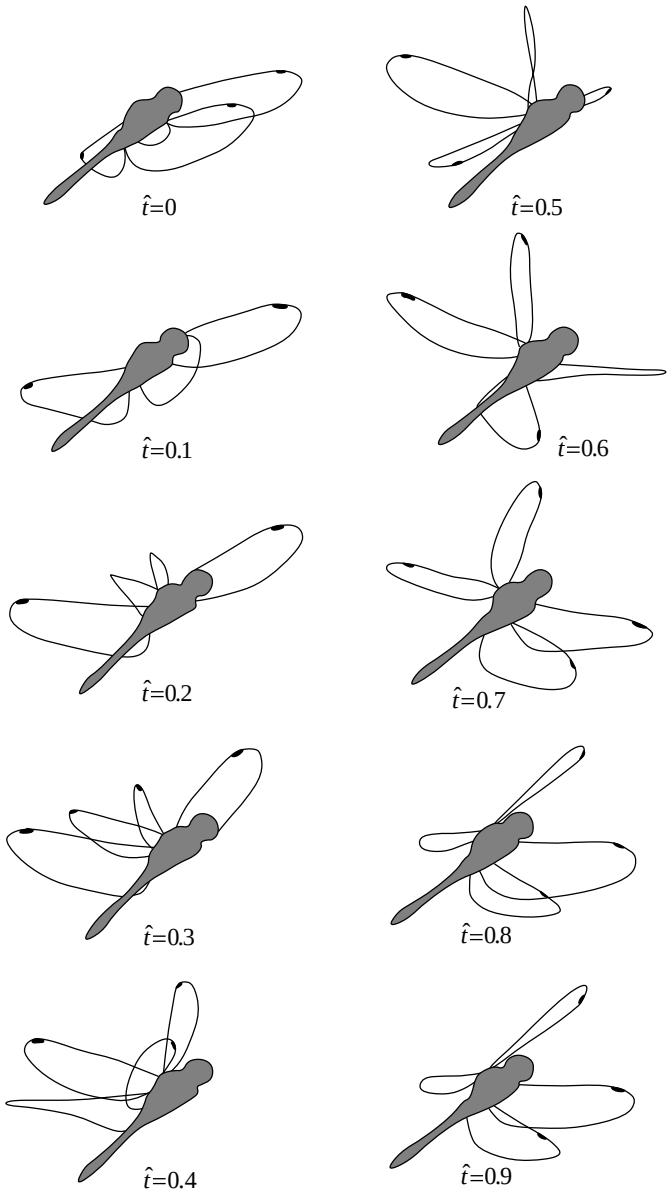

Fig. 4. Silhouette images of *Sympetrum sanguineum* from the wingbeat SSan6.1 (Fig. 7E). Time $\hat{t}$ is normalised by the forewing period.

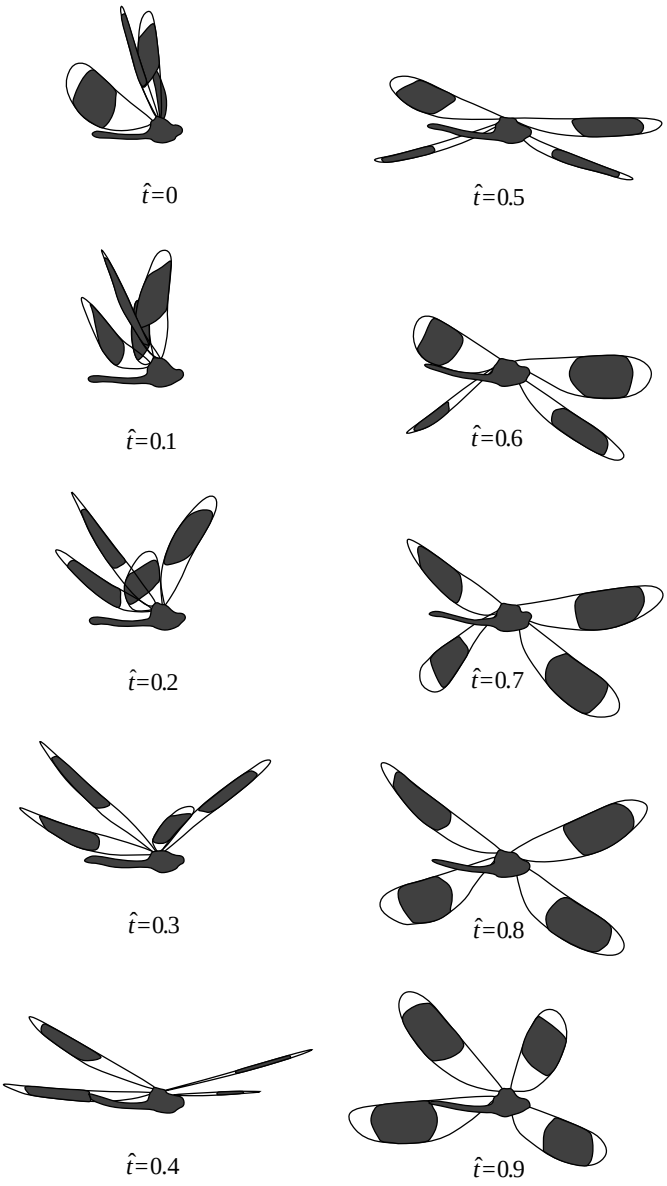

Fig. 5. Silhouette images of *Calopteryx splendens* from the wingbeat CS1.3 (Fig. 8B). Time $\hat{t}$ is normalised by the forewing period.

length R_f. The circle is horizontal, but is viewed from above for this drawing. Four complete spokes are drawn within the circle at 90° intervals. The spokes pass through the centre of mass of the dragonfly. The thicker spokes lie in the sagittal plane, with the arrow facing in the forward direction. A further eight marks around the inside of the circle indicate 30° divisions. The body is drawn to scale, and the angle between the body and the forward direction spoke is the mean body angle $\overline{\chi}$. The non-dimensional velocity $\hat{V}$ is drawn as a thick brown line with a solid arrowhead, whilst the non-dimensional acceleration $\hat{A}$ is drawn as a thick green line with an open arrowhead. The velocity and acceleration vectors start at the centre of mass and are drawn along the hypotenuses of right-angled triangles, with the other two sides being horizontal and vertical. Both vectors are drawn to scale, and at the correct inclination ξ and yaw ψ; angles ξ and ψ are illustrated in Fig. 7A. Values for $\hat{V}$, $\hat{A}$, ξ and ψ are given for each sequence. The velocity V and acceleration A can be calculated from $\hat{V}$ and $\hat{A}$ using the mean forewing length R_f, the mean wingbeat frequency n [=(n_f+n_h)/2] and equations 4 and 5.

The lower drawings in Figs 7 and 8 show a side view of the dragonfly with the respective wingtip positions during a wing stroke. Points for the forewing tip are marked as blue circles, while points for the hindwing tip are marked as red diamonds. The stroke planes for the fore- and hindwing pairs are at angles β_f and β_h to the horizontal, respectively. The stroke planes are indicated by the pairs of coloured arrows and pass through their respective wingbases, each denoted by a cross. The distance from the wingbase to the tip of each stroke plane arrow denotes

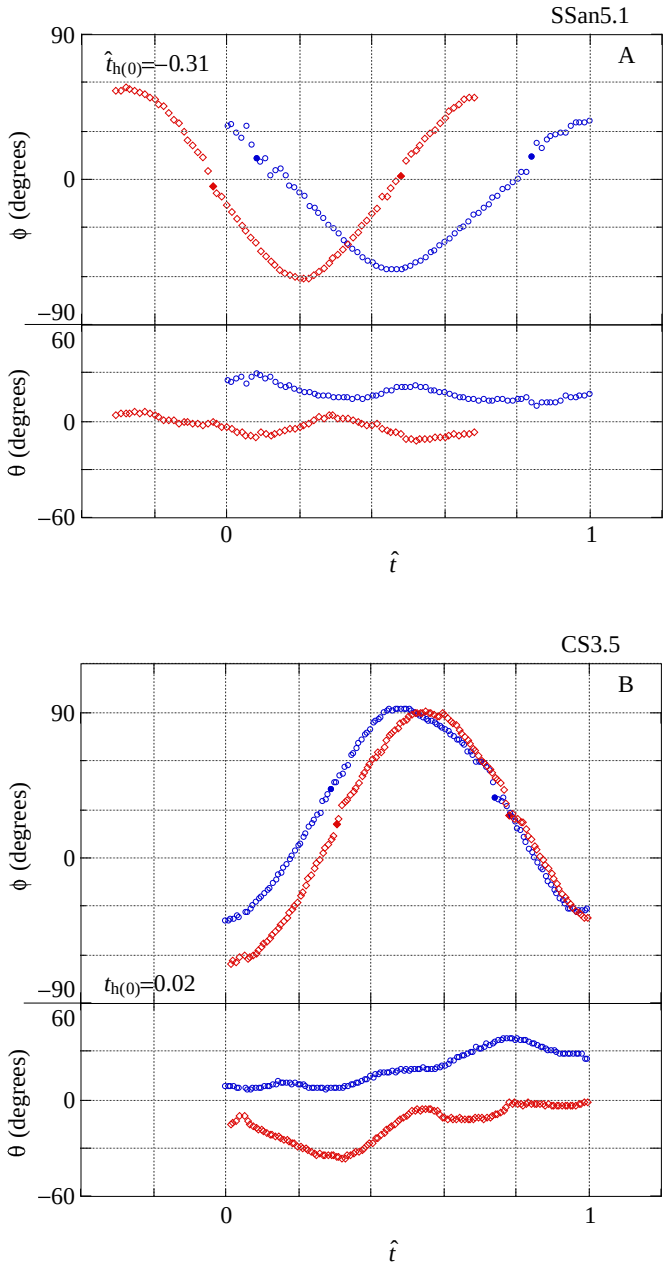

Fig. 6. Time series for the positional angle of the wing within the stroke plane ϕ and perpendicular to that plane θ. Blue circles denote positions for the forewings, whilst red diamonds are for the hindwings. Filled symbols indicate where the wing passes through the *y*,*z* plane, and thus where the maximum projected wing length occurs. The hindwing sequence starts at time $\hat{t}_{h(0)}$ relative to the forewing. Non-dimensional time $\hat{t}$ is defined in equation 10. (A) *S. sanguineum* flight SSan5.1. (B) *C. splendens* flight CS3.5.

the wing length *R* for that particular wing pair. The length of each stroke plane arrow denotes the mean chord $\bar{c}$ for the respective wings. The body is shown at the mean body angle $\bar{\chi}$ and is also drawn to scale.

The wingtip path is given by the coloured symbols. These points represent the projected positions of the wingtip onto the x',z' plane; i.e. they indicate where the wing tips would be seen if viewed from the side. Black arrows show the direction of travel for the wingtips. Values are given for the stroke plane angle β, the stroke amplitude Φ, the mean positional angle $\bar{\phi}$ of the stroke, and the roll angle η for each wing pair. The angles between the velocity and acceleration vectors and the normal to the stroke plane, κ_V and κ_A, respectively, are also given for each wing pair. Values presented for Φ and $\bar{\phi}$ are calculated from the Fourier series, which are discussed below.

The period for the forewing beat is scaled to non-dimensional time $\hat{t}$, where:

$$\hat{t} = n_f t\,, \tag{10}$$

and so for the forewings $0<\hat{t}<1$. In this same $\hat{t}$ scale, the stroke period for the hindwings is not necessarily 1. The start of the hindwing cycle relative to that of the forewing is $\hat{t}_{h(0)}$ and is in the $\hat{t}$ scale. The fore- and hindwing beat cycles were not always digitised from equivalent positions, so $\hat{t}_{h(0)}$ does not necessarily represent a hindwing phase shift. This phase shift can be visualised by reconstructing the Fourier series for both wing pairs with the hindwing cycle commencing at $\hat{t}_{h(0)}$. The advance ratio *J* is given by:

$$J = \frac{V}{2\Phi n R}\,. \tag{11}$$

The respective fore- and hindwing beat frequencies, n_f and n_h, and the ratio of the downstroke to upstroke duration *d*/*u* are also given in Figs 7, 8.

Fourier series analysis of the kinematics

Coefficients *a*, c_i and o_i, as fitted by the Fourier series to the ϕ and θ data (see equation 7), are presented in Tables 2 and 3. The standard errors for the predicted curves with each additional level of harmonics (as calculated by equation 8) are also given. The Fourier series for ϕ show that the fundamental (*i*=1) dominates the curve, with the second harmonic typically more important than the higher harmonics.

An inherent problem with this type of analysis is a subjective element in digitising the wingtips. The wingtip is not well-defined for some wing orientations, and its perceived position may change as the wings move. Furthermore, as the wingtips reappear on the far side of the body silhouette, a different position for the tip may be chosen. These problems were especially noticeable for the θ data as it was often harder to judge the chordwise location of the wingtip than the spanwise location. The higher harmonics of the Fourier series give a better fit to the data where these discontinuities occur, but smaller standard errors do not necessarily reflect a better goodness of fit. Curves using the first four harmonics describe the data well without producing unrealistic kinks, whereas by the fifth harmonic kinks are introduced into the fits around the regions of digitising uncertainty.

Flight descriptions

When describing the flights of *S. sanguineum* or *C. splendens*, it must be remembered that the data for each species contain measurements from a number of different individuals.

Table 2. *Fourier coefficients and standard errors of the Fourier series for ϕ and θ for* Sympetrum sanguineum

	a	c_i					o_i					S.E.M.				
SSan	0	1	2	3	4	5	1	2	3	4	5	1	2	3	4	5
ϕ																
2.1f	14.51	43.48	0.98	1.02	1.32	0.39	5.40	283.07	358.21	254.47	315.63	2.68	2.62	2.55	2.36	2.37
2.1h	–7.49	44.97	3.93	1.71	1.91	0.41	353.69	245.47	339.70	237.66	180.19	3.90	2.70	2.42	1.99	2.00
2.3f	1.08	46.30	5.10	2.90	2.65	3.36	186.35	65.35	132.26	104.70	125.22	3.67	2.15	1.74	2.24	3.01
2.3h	–28.55	41.94	2.39	2.54	1.06	0.84	196.73	301.99	188.83	358.77	153.95	2.98	2.46	1.62	1.45	1.33
5.1f	–25.28	42.24	2.19	3.19	0.84	0.42	190.52	354.32	229.83	47.52	152.85	3.59	3.22	2.23	2.17	2.17
5.1h	–4.29	56.87	2.52	0.94	0.68	0.87	170.21	244.71	123.14	159.83	147.95	2.35	1.52	1.38	1.31	1.15
5.2f	–17.71	31.09	3.08	1.11	0.50	1.05	351.99	307.77	31.51	101.90	99.41	3.43	2.64	2.57	2.58	2.50
5.2h	–9.26	44.90	2.45	1.76	0.61	0.60	358.61	244.74	64.78	25.06	325.04	3.04	2.50	2.18	2.16	2.15
6.1f	–3.13	49.44	4.04	3.79	4.54	4.20	353.50	226.96	328.84	173.42	344.63	3.31	1.81	2.27	3.54	4.59
6.1h	–16.55	53.76	4.72	1.72	1.34	0.96	341.11	214.64	77.85	274.94	67.70	4.16	2.36	2.03	1.80	1.67
6.2f	9.89	45.96	3.29	1.07	0.41	0.64	7.60	63.34	50.97	152.96	303.10	3.29	2.33	2.23	2.24	2.22
6.2h	–9.14	53.76	2.14	1.77	0.28	0.75	4.50	295.97	24.06	50.61	73.41	2.70	2.27	1.88	1.90	1.84
9.1f	9.68	44.84	2.31	0.51	0.95	0.57	88.83	71.41	269.56	248.76	245.35	4.09	3.78	3.82	3.80	3.83
9.1h	–3.55	47.36	6.38	3.36	1.22	0.81	264.39	254.86	117.35	82.78	334.52	6.06	4.01	3.24	3.16	3.13
θ																
2.1f	29.34	0.53	2.63	0.79	0.81	0.82	70.89	259.43	73.56	13.11	137.05	2.46	1.59	1.52	1.40	1.27
2.1h	–11.45	1.70	1.45	0.62	1.19	0.25	267.33	231.18	10.74	44.20	203.77	1.88	1.59	1.55	1.29	1.30
2.3f	34.24	1.41	3.84	0.40	0.55	0.85	235.15	249.44	296.41	278.64	289.39	2.97	1.36	1.40	1.48	1.62
2.3h	–14.33	1.41	3.31	1.84	1.61	0.87	138.27	228.94	345.02	123.12	33.99	3.37	2.37	1.97	1.59	1.48
5.1f	35.40	3.30	5.03	2.05	1.53	0.48	109.06	309.75	59.50	292.26	52.91	4.24	2.25	1.71	1.30	1.27
5.1h	–6.36	1.68	6.33	1.48	1.65	0.78	92.25	274.62	167.63	285.34	74.03	5.07	2.30	2.06	1.69	1.61
5.2f	30.94	3.27	1.64	1.55	0.98	0.16	81.79	296.08	173.33	266.87	213.65	1.92	1.54	1.09	0.84	0.85
5.2h	–3.96	6.62	4.37	1.71	1.44	1.09	83.63	292.56	106.67	281.90	101.12	3.85	2.26	1.91	1.61	1.41
6.1f	36.45	1.50	4.20	0.66	1.34	2.73	77.62	196.51	286.17	41.44	175.55	3.22	1.39	1.35	1.43	2.10
6.1h	–4.31	2.59	1.95	0.54	1.40	0.72	71.34	234.29	171.20	307.75	130.39	2.03	1.52	1.47	1.03	0.88
6.2f	33.43	2.16	5.20	1.20	1.34	0.95	89.71	271.03	71.87	304.80	87.34	4.36	2.29	2.15	1.94	1.83
6.2h	–3.98	3.30	4.65	0.93	1.26	0.70	93.96	273.00	78.09	339.01	112.83	3.83	1.92	1.82	1.58	1.51
9.1f	38.91	0.72	4.93	1.14	1.32	0.51	40.10	134.55	31.46	22.49	329.57	4.12	2.19	2.07	1.87	1.86
9.1h	–3.18	0.74	3.24	0.77	0.31	0.59	311.75	28.83	54.36	326.17	263.89	2.88	1.75	1.69	1.69	1.64

All units are in degrees. a, c_i and o_i are defined in equation 7.
See text for further details.

There were no cases in which two individuals flew with the same velocity and acceleration, and so there is no way of assessing the variation between individuals. The problem of a comparative description of the flight of each species is confounded by the fact that the flights were at different velocities and accelerations. Past studies have concentrated on steady flight, in which there is no acceleration and in which the thrust is predominantly used for weight support and thus is reasonably constant. The flights filmed in the present study were totally unrestrained and showed a threefold range of thrust and velocity.

The precise nature of any changes in the kinematic parameters with velocity and thrust is unknown. Indeed, a major objective of this study was to discover such trends. Preliminary examination of the results showed that relationships more complicated than linear could not be justified. It was therefore decided to test whether each kinematic parameter changed with velocity and thrust using simple least-squares linear regression, i.e. whether the slope was significantly different from zero. The purpose of fitting linear regression lines to the data is only to identify trends and not to estimate a functional relationship; as such, it was deemed inappropriate to record the equations for the regression lines. For the purposes of discussion, regressions are deemed significant at a 95% confidence level. However, to clarify trends in Figs 9 and 10, regression lines are distinguished at a 90% confidence level, and this confidence level is deemed 'good' in the text.

Table 4 gives the mean values and ranges for the kinematic parameters. Some of the regressions against velocity and thrust are shown in Figs 9 and 10. The significance of the trends are indicated in Table 5.

Flight of Sympetrum sanguineum

Sympetrum sanguineum faces its flight direction, with its body at a nose-up attitude to the horizontal. All flights were ascending, and the mean body angle shows a significant linear regression with the angle of inclination of the velocity (Fig. 9), giving a mean body angle 31° shallower than the inclination of the flight velocity.

Table 3. *Fourier coefficients and standard errors of the Fourier series for ϕ and θ for* Calopteryx splendens

	a	c_i					o_i					S.E.M.				
SSan	0	1	2	3	4	5	1	2	3	4	5	1	2	3	4	5
ϕ																
1.1f	28.47	59.13	3.25	1.24	1.71	0.19	14.36	71.64	46.25	56.11	72.83	3.70	2.85	2.74	2.49	2.51
1.1h	18.47	54.99	3.44	2.78	3.41	3.64	6.50	93.82	3.51	191.91	49.32	3.10	2.68	2.81	3.27	4.08
1.3f	53.95	54.89	4.88	0.55	1.64	0.57	153.82	35.29	191.90	1.72	189.50	4.13	2.19	2.16	1.81	1.77
1.3h	27.99	57.49	3.42	2.35	0.81	0.82	158.90	350.02	109.74	31.61	137.08	3.95	3.14	2.68	2.62	2.56
2.2f	47.36	48.67	5.44	1.06	0.75	0.82	163.13	63.18	176.14	35.73	296.10	4.35	1.97	1.82	1.75	1.66
2.2h	31.14	51.13	2.26	0.52	1.17	0.48	166.69	44.79	184.17	5.31	150.30	2.37	1.74	1.70	1.49	1.45
2.3f	27.4	68.13	8.12	3.45	2.09	1.63	348.43	62.77	314.15	60.42	265.92	7.58	4.93	4.29	4.05	3.90
2.3h	–14.3	49.79	1.92	2.5	1.72	1.51	354.05	312.76	359.49	331.63	313.43	3.27	3.01	2.42	2.18	2.03
2.5f	33.43	61.22	1.64	0.34	0.99	0.77	7.17	60.92	170.06	208.86	72.56	2.25	1.94	1.94	1.81	1.73
2.5h	5.84	55.04	2.58	1.82	1.45	1.41	340.21	333.57	308.01	55.93	92.66	3.48	2.97	2.68	2.49	2.28
3.2f	45.25	67.14	4.08	2.55	0.95	1.96	2.98	153.94	202.64	63.48	260.09	4.15	2.82	2.36	2.38	2.22
3.2h	31.38	74.09	5.63	1.08	0.9	0.14	1.27	198.89	218.72	206.48	296.65	4.75	2.52	2.42	2.34	2.36
3.3f	85.63	70.64	18.21	2.8	0.42	2.74	231.02	290.42	296.78	214.15	233.67	13.58	4.09	3.52	3.51	2.78
3.3h	79.05	68.32	20.01	2.73	1.28	0.58	239.94	314.59	8.44	101.26	245.95	14.53	2.86	2.10	1.90	1.87
3.5f	61.7	63.09	3.43	2.33	0.99	0.39	354.08	153.21	64.70	92.87	60.43	3.38	2.34	1.65	1.50	1.49
3.5h	41.87	70.75	4.83	3.37	1.69	1.88	339.38	113.49	290.95	122.23	293.90	5.48	4.34	3.66	3.48	3.23
4.2f	69.5	37.2	3.73	0.37	1.73	1.52	159.96	311.94	180.96	51.70	124.37	4.93	4.17	4.19	4.03	3.91
4.2h	27.48	43.37	3.82	2.23	2.40	0.29	160.91	18.63	129.96	317.83	177.72	5.09	4.30	4.02	3.66	3.69
θ																
1.1f	53.5	6.32	6.6	1.74	1.29	0.46	287.61	135.01	47.78	147.67	66.45	5.06	1.80	1.29	0.90	0.84
1.1h	–29.4	7.73	1.82	1.55	1.54	1.99	275.49	353.55	43.97	111.32	57.98	2.41	1.99	1.64	1.41	1.40
1.3f	40.75	0.72	3.06	1.81	0.29	0.19	218.97	196.21	151.50	316.59	245.82	2.65	1.53	0.81	0.79	0.78
1.3h	–28.3	4.57	3.71	2.47	1.99	0.48	77.48	268.80	139.79	56.38	240.25	3.92	2.91	2.31	1.81	1.79
2.2f	36.82	0.73	3.7	0.91	0.55	0.58	208.39	216.16	113.11	331.15	133.59	2.93	1.31	1.13	1.07	0.98
2.2h	–27.6	2.51	3.46	0.96	0.19	0.08	86.41	306.42	173.36	343.04	221.28	2.77	1.24	1.03	1.02	1.03
2.3f	43.47	3.05	5.07	1.36	0.45	0.33	67.60	221.02	303.78	2.99	305.25	3.85	1.31	0.89	0.83	0.80
2.3h	–31.2	3.23	1.89	1.53	0.36	1.05	77.55	329.01	3.22	171.60	47.69	2.25	1.83	1.45	1.44	1.23
2.5f	43.64	7.24	1.02	0.69	1.13	0.74	281.08	303.92	144.30	113.21	281.11	1.70	1.55	1.48	1.24	1.12
2.5h	–32	8.89	3.8	1.54	0.62	0.32	256.40	322.33	1.36	74.14	290.94	3.16	1.63	1.21	1.13	1.12
3.2f	39.75	3.00	1.01	1.69	1.19	0.45	277.29	263.04	34.38	90.83	264.53	1.88	1.76	1.29	0.88	0.72
3.2h	–21.7	7.80	7.12	0.64	1.64	0.96	287.75	17.93	261.36	56.04	271.81	5.45	1.90	1.86	1.44	1.26
3.3f	66.27	4.39	11.89	5.01	1.16	2.84	132.67	267.44	355.94	119.07	76.25	9.41	4.74	3.22	3.1	2.29
3.3h	–17.60	6.77	7.42	1.58	1.47	1.16	176.01	220.75	180.60	167.27	74.45	5.84	2.49	2.24	1.98	1.81
3.5f	38.66	13.81	4.21	1.83	2.26	1.45	266.41	120.66	356.44	80.90	252.44	4.24	3.07	2.81	2.33	2.10
3.5h	–31.5	13.70	6.13	2.94	1.31	0.61	256.92	4.94	347.40	346.80	128.73	5.18	2.79	1.81	1.56	1.50
4.2f	58.91	3.72	1.70	1.30	1.32	0.85	76.62	201.11	141.78	261.43	44.15	2.34	1.98	1.79	1.53	1.40
4.2h	–22.3	5.49	2.85	0.81	0.62	0.53	72.85	276.58	174.08	305.89	150.64	2.38	1.25	1.10	1.01	0.94

All units are in degrees. a, c_i and o_i are defined in equation 7.
See text for further details.

The stroke planes are approximately perpendicular to the direction of the velocity; the mean angle between the normals to the stroke planes and the direction of the velocity was 16° for both fore- and hindwings. Significant linear regressions for these angles, κ_{fV} and κ_{hV}, with the flight velocity show that as V increases the stroke planes tilt to face the direction of the velocity more closely. The normals to the stroke planes are also kept close to the direction of the thrust T, with the angles κ_{fT} and κ_{hT} between the normals to the stroke planes and the thrust direction taking mean values of 19° (Table 4).

The stroke planes are at fixed angles relative to the thorax, with the angles between the stroke planes and the longitudinal body axis being 48° and 50° for the fore- and hindwings, respectively; a matched-pair t-test showed that there was no significant difference between these angles. As the body inclination increases for climbing flight, the stroke planes flatten out relative to the horizontal, facing a more vertical direction.

The hindwing shows a greater stroke amplitude Φ than the forewing; this difference is due to the hindwing reaching a lower position ϕ_{min} than the forewing. The upper position of the stroke, ϕ_{max}, is similar for the two wings. The midpoint of the forewing stroke, $\bar{\phi}_f$, is approximately 6° higher on average than for the hindwing, $\bar{\phi}_h$, and so the forewings beat around a more dorsal position within their stroke plane than do the hindwings. Both the fore- and hindwings show a general

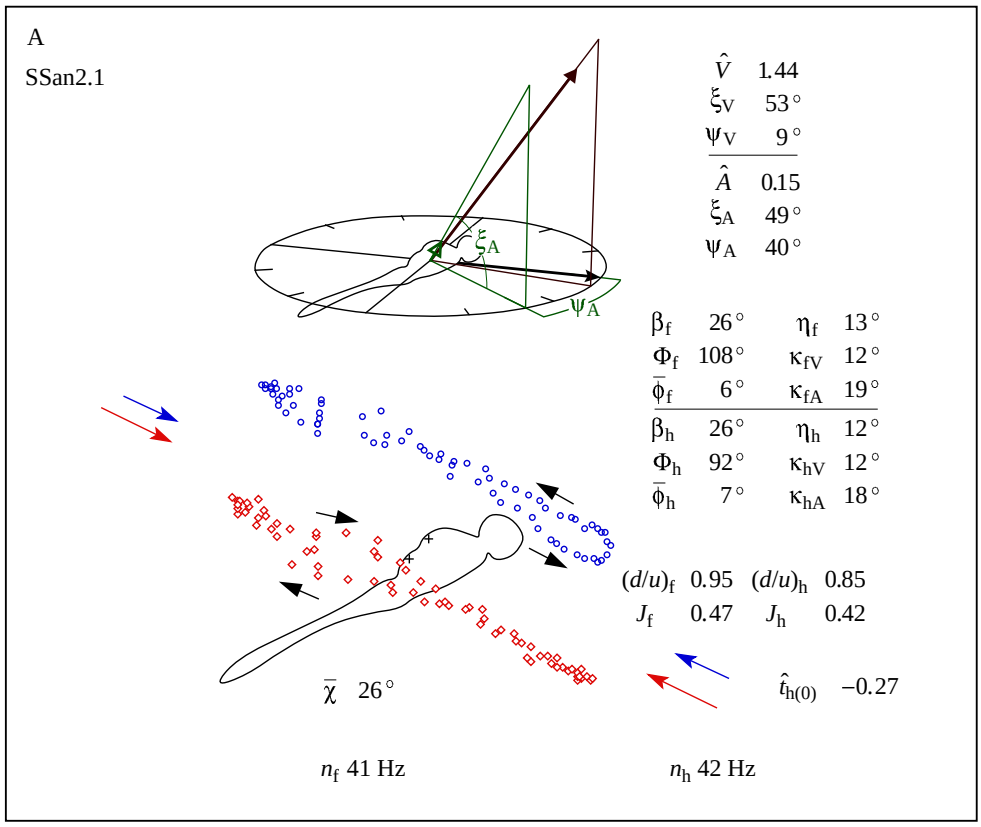

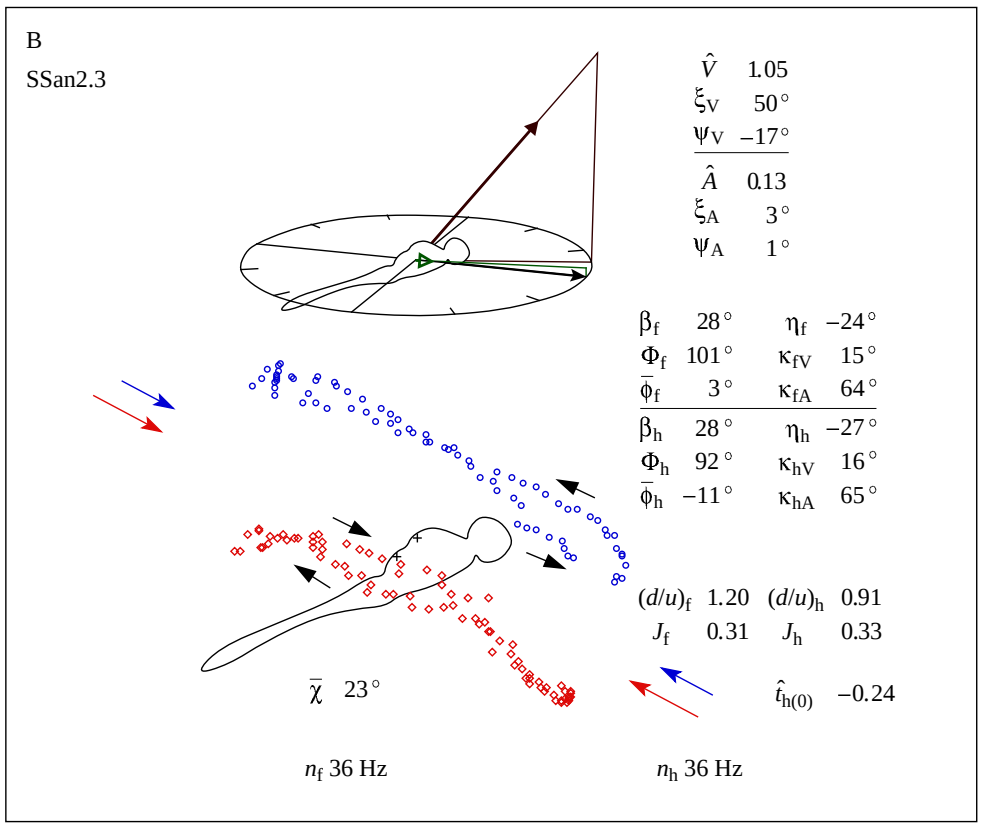

Fig. 7A,B. For legend see p. 571

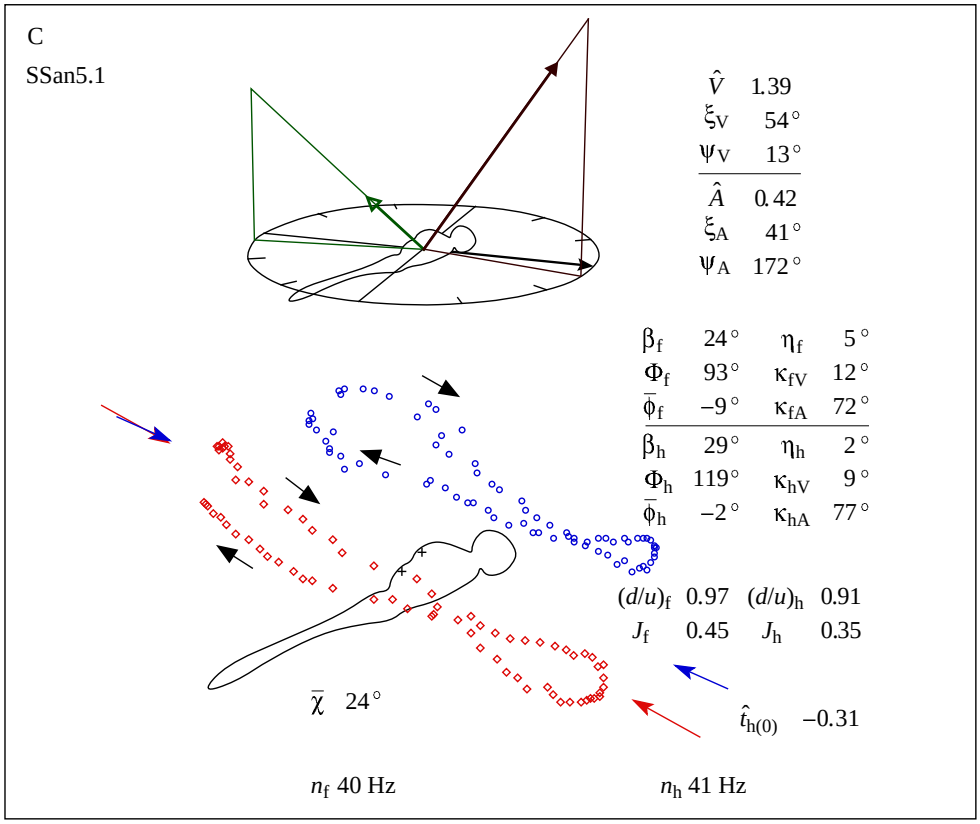

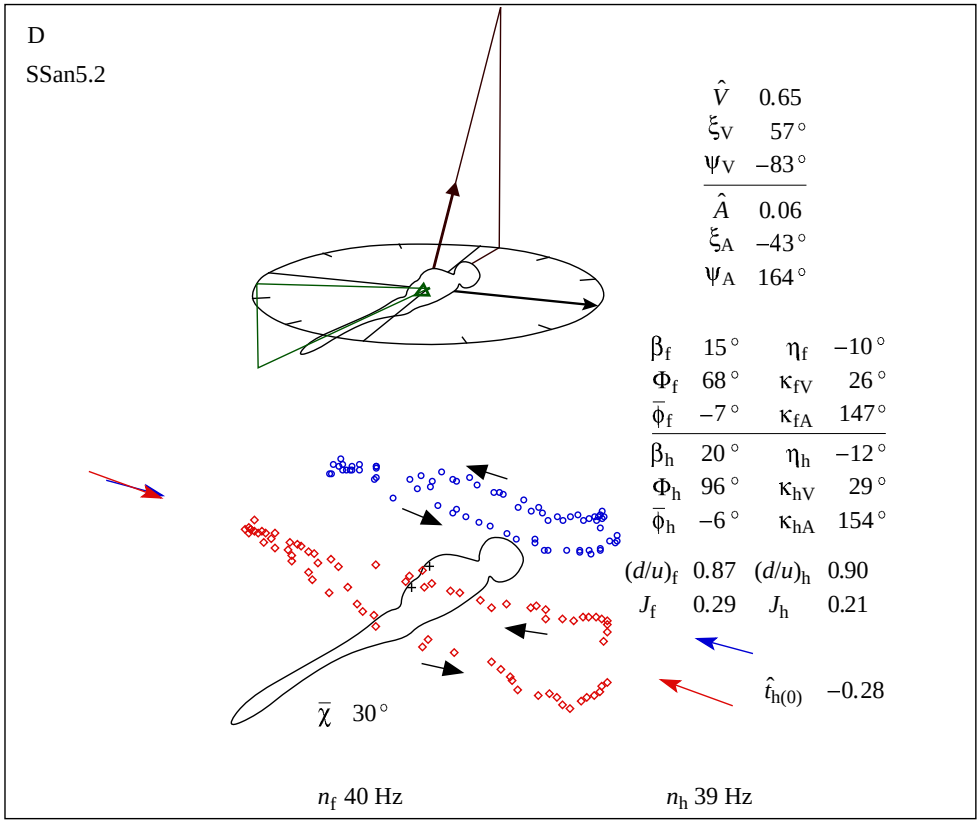

Fig. 7C,D. For legend see p. 571.

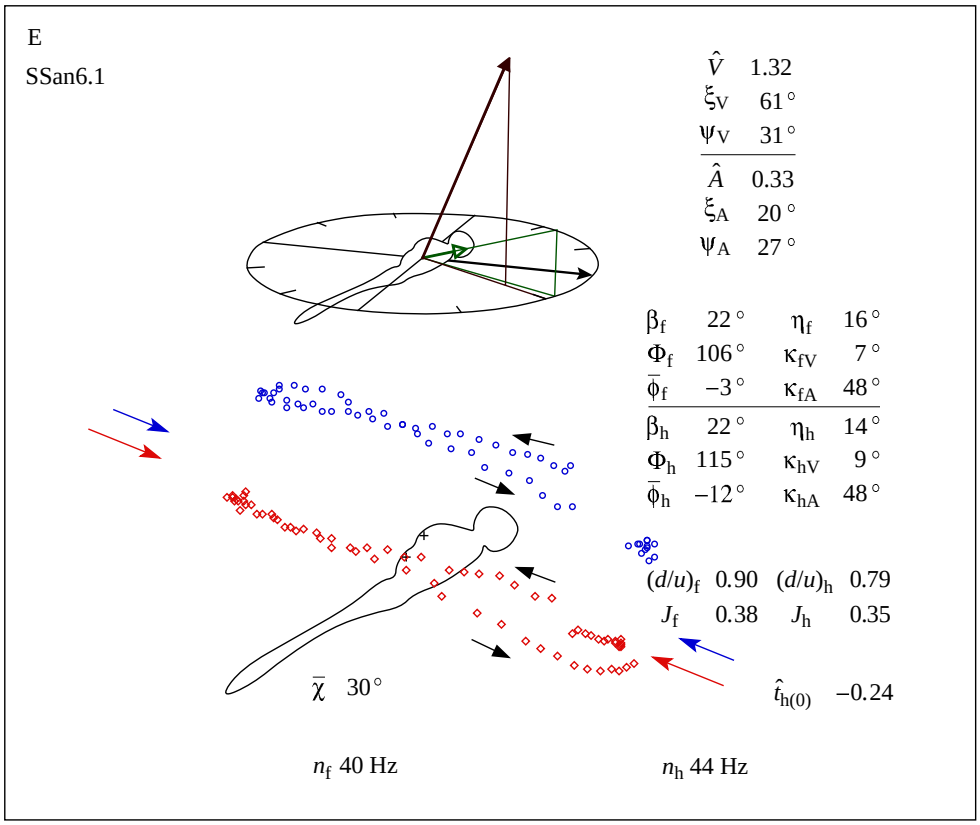

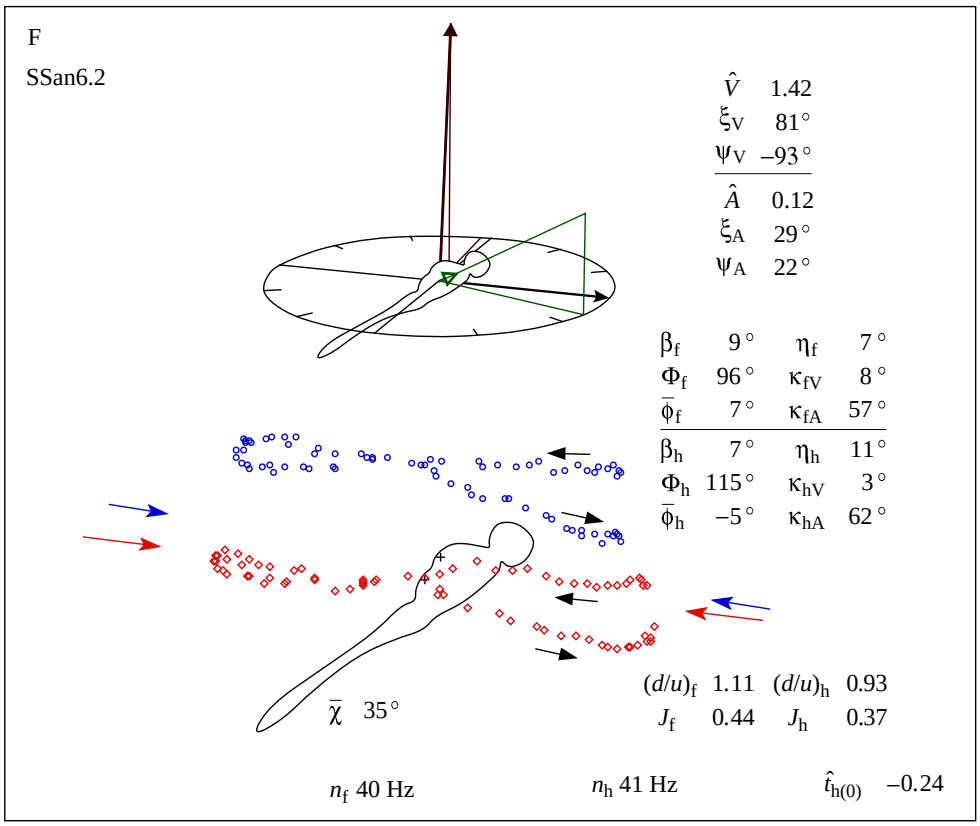

Fig. 7E,F. For legend see p. 571.

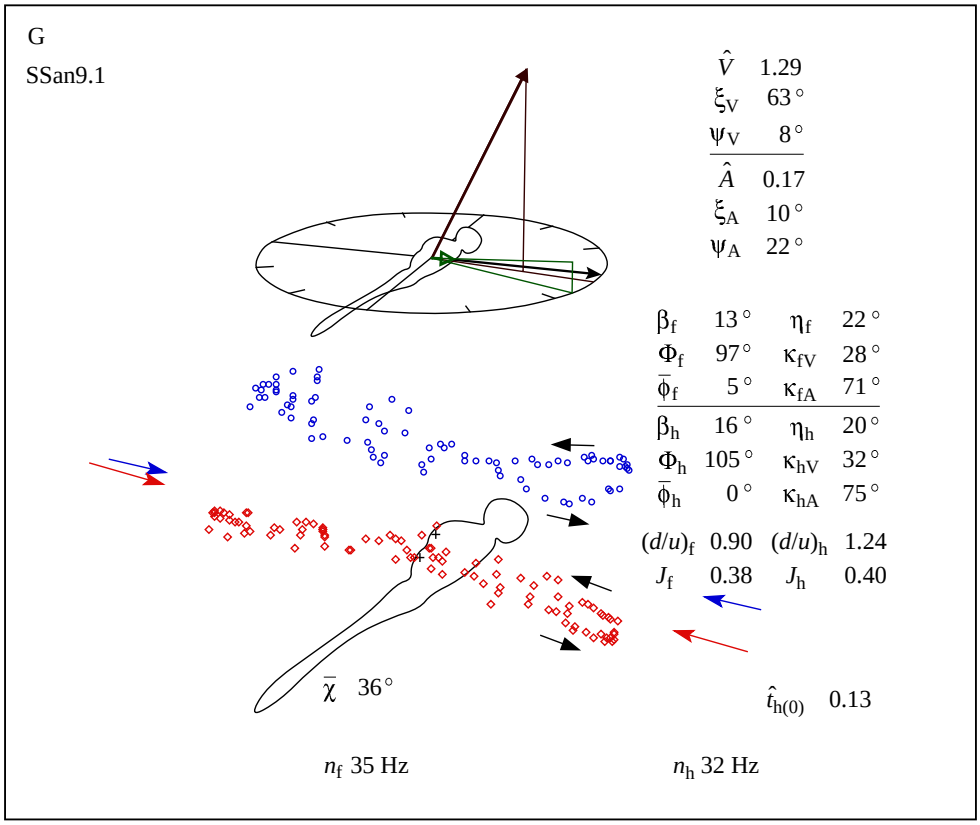

Fig. 7. (A–G) The analysed wingbeats for *Sympetrum sanguineum*, showing the vectors for non-dimensional velocity and non-dimensional acceleration (upper drawings), and the reconstructed wingtip path (lower drawings). Full details of these diagrams along with definitions of the parameters can be found in the text.

increase of Φ with V. Only the hindwing shows a good regression of Φ_h with T (Fig. 10), mainly due to increases in $\phi_{h,max}$; the only good trend for the forewings with T, in contrast, is the decrease of $\phi_{f,min}$ with increasing T.

The wingbeat frequency n remained reasonably constant for all the flights, with a mean value of 39 Hz for both the fore- and hindwings. There was no significant regression of n with either V or T. The downstroke-to-upstroke ratios d/u were 0.98 and 0.93 for the fore- and hindwings, respectively, but a matched-pair t-test showed there to be no significant difference between these values. The forewing motion lagged behind that of the hindwing in all sequences by approximately 26 % of the forewing period, i.e. a 94 ° phase lag (Fig. 6A).

The mean flapping velocity $2n\Phi R$ was 14 % higher for the hindwings than for the forewings. There was a greater variance in Φ_f than in Φ_h, and less variance in n_f than in n_h, but the variance for the mean flapping velocity was greatest for the hindwings. Changes in the aerodynamic output of the wings may be due more to changes in hindwing motion than to changes in forewing motion.

Flight of Calopteryx splendens

Calopteryx splendens faces its flight direction and does not raise its body inclination to meet the inclination of the velocity. Nearly half the flights had a horizontal body posture, whilst the body varied between head-down and head-up inclinations for the others. The mean body angle did not show any significant linear regression with the inclination of velocity (Table 5).

The wing motion is more variable than for *S. sanguineum*; the angle between the stroke plane and the body axis is more variable and θ deviated more from the stroke plane. Angles between the normals to the stroke planes and the direction of velocity are greater than for *S. sanguineum*, but the angles to the thrust vectors were similar. The normals to the stroke planes were at mean angles of 31 ° and 22 ° from the velocity direction for the fore- and hindwings, respectively, and 21 ° from the thrust direction for both. β_h shows a significant linear relationship with the inclination of velocity but not with the mean body angle. There were also no significant regressions for κ_{fV} and κ_{hV} with velocity, nor were there significant regressions for κ_{fT} and κ_{hT} with thrust. The stroke planes do not tilt to face V or T more closely as these parameters increase.

Both the fore- and hindwings beat through a similar amplitude Φ of approximately 120 °, and this amplitude is considerably greater than that for *S. sanguineum*. A matched-pair t-test showed that $\bar{\phi}_f$ was systematically approximately 12 ° greater than $\bar{\phi}_h$, with the forewings beating around a more dorsal position, similar to the dragonfly. The forewings normally come close together at the top of their stroke, with a mean of 83 ° for $\phi_{f,max}$, and they show little variation in $\phi_{f,max}$.

Table 4. *Kinematic parameters for the analysed flights*

	Sympetrum sanguineum		*Calopteryx splendens*	
V ($m\,s^{-1}$)	1.31±0.13 (0.70, 1.66)		0.94±0.14 (0.49, 1.66)	
A ($m\,s^{-2}$)	8.39±2.25 (2.62, 18.33)		5.76±0.56 (2.69, 8.28)	
T (mN)	1.93±0.29 (1.11, 3.46)		1.34±0.10 (0.96, 1.93)	
$\hat{V}$	1.22±0.11 (0.65, 1.44)		1.59±0.22 (0.61, 2.38)	
$\hat{A}$	0.20±0.05 (0.06, 0.42)		0.52±0.07 (0.12, 0.92)	
$\hat{T}$	1.59±0.24 (0.85, 2.65)		1.30±0.08 (0.79, 1.59)	
$\bar{\chi}$ (degrees)	29.1±1.97 (22.6, 35.7)		4.8±3.10 (–5.0, 25.2)	
	Forewings	Hindwings	Forewings	Hindwings
n (Hz)	38.7±0.82 (35.3, 40.8)	39.2±1.61 (31.6, 44.4)	19.9±1.21 (14.1, 27.1)	20.3±1.26 (13.7, 27.1)
β (degrees)	19.3±2.66 (8.8, 27.9)	21.1±2.92 (7.0, 28.6)	17.0±3.53 (–6.1, 28.9)	28.1±3.95 (7.8, 51.6)
Φ (degrees)	90.5±4.95 (64.1, 107.0)	101.56±3.92 (88.5, 115.8)	120.1±7.51 (74.8, 147.7)	121.0±6.95 (91.8, 148.3)
ϕ_{max} (degrees)	45.3±4.12 (25.3, 54.4)	44.89±3.24 (30.3, 55.6)	83.4±8.30 (73.9, 99.7)	72.3±5.05 (46.6, 93.2)
$\bar{\phi}$ (degrees)	0.1±2.68 (–10.8, 7.3)	–5.89±1.79 (–14.0, –0.2)	23.4±2.50 (13.9, 38.4)	11.8±2.69 (–5.6, 21.0)
ϕ_{min} (degrees)	–45.2±3.11 (–56.9, –37.2)	–56.7±1.89 (–63.7, –51.4)	–36.7±5.75 (–58.9, –1.0)	–48.7±3.61 (–62.9, –30.0)
$\bar{\theta}$ (degrees)	17.1±0.61 (14.7, 19.5)	–3.4±0.82 (–7.2, -1.6)	23.4±1.71 (18.4, 33.1)	–13.4±0.85 (–16.0, –8.8)
d/u	0.98±0.05 (0.87, 1.20)	0.93±0.05 (0.79, 1.24)	1.09±0.04 (0.7, 1.2)	1.01±0.04 (0.75, 1.14)
κ_V (degrees)	15.5±3.09 (7.3, 27.8)	15.8±4.14 (3.4, 32.4)	30.5±5.01 (10.8, 59.4)	21.6±3.35 (8.3, 42.4)
κ_T (degrees)	19.3±5.54 (2.4, 37.2)	18.5±5.54 (4.0, 39.8)	21.9±3.66 (4.7, 33.5)	21.0±3.27 (6.1, 31.1)

Values are given as mean ± S.E.M. (minimum value, maximum value).

All variables are defined in the text.

The hindwings beat to a lower position $\phi_{h,min}$ than the forewings, but most of the variation of the stroke occurs dorsally. The lower mean $\phi_{h,max}$ of 72° gives the hindwings more room for manoeuvre at their dorsal extreme, and they do indeed show a greater range of $\phi_{h,max}$. The hindwing stroke amplitude Φ shows a good regression (P<0.01) with V, but there are no notable trends linking any parameter for stroke position with T.

Flight CS3.3 (Fig. 8G) was atypical of damselfly flights and is an example of 'threatening' flight (Rüppell, 1985), where all four wings are briefly held together motionless at the top of the stroke. If this unusual, more ballistic, flight of CS3.3 (at T=0.96×10^{-3} N) were to be ignored, then there is a significant increase in $\phi_{h,max}$ with increasing thrust (P=0.029).

The mean wingbeat frequency n was 20 Hz for both the fore- and hindwings, half the frequency of the *S. sanguineum* wingbeats. There was no significant regression of n with V. There was, however, a good regression of n with T. The downstroke-to-upstroke ratios d/u were 1.09 and 1.01 for the forewings and hindwings, respectively, but a matched-pair t-test showed there to be no significant difference in these values. The downstroke duration was slightly longer than that of the upstroke, which is opposite to the situation for *S. sanguineum*. The forewing motion was advanced by 8% of its period relative to the hindwing, i.e. a 29° phase advance (Fig. 6B); again, this is in contrast to the phase lag of *S. sanguineum*.

A matched-pair t-test showed that the mean flapping velocities of the fore- and hindwings, $2n\Phi R$, were not significantly different from each other. If the clap-and-fling mechanism enhances the lift generated by a wing pair, and the magnitude of this enhancement is a function of the proximity of the wings when they fling apart, then the forewings of *C. splendens* must generate more lift than the hindwings. The hindwings, however, reach a more variable position at the top of their stroke and are used for controlling the total thrust from the wing system.

Discussion

General flight remarks

The mean velocity for the dragonflies was faster than that for the damselflies: however, the maximum velocity of 1.66 $m\,s^{-1}$ was the same for both species. During gliding (Wakeling and Ellington, 1997*a*), a higher maximum velocity of 2.6 $m\,s^{-1}$ was recorded for *S. sanguineum*, which was faster than the maximum for *C. splendens*. Neither experimental set-up was designed for eliciting maximum velocities, and it is unlikely that these values are the maximum possible by these insects. However, the values are similar to the maximum reported velocities of dragonflies in the field. Field velocities of dragonflies show a tendency to increase with increasing body mass (data from Rüppell, 1989); for the smaller dragonflies the velocities are: *Epitheca cynosura* (175 mg) 2 $m\,s^{-1}$, *Micrathyria atra* (214 mg) 3 $m\,s^{-1}$ (May, 1991), *Sympetrum danae* (105 mg) 4 $m\,s^{-1}$, and *C. splendens* (118 mg) 1.9 $m\,s^{-1}$ (Rüppell, 1989).

Both the mean and the maximum accelerations of *S. sanguineum* were higher than those for *C. splendens*. The respective maximum accelerations, 18.33 $m\,s^{-2}$ and 8.28 $m\,s^{-2}$, again fall into the range of those previously measured for free-flying dragonflies: *E. cynosura* 11.8 $m\,s^{-2}$, *M. atra* 15.9 $m\,s^{-2}$ (May, 1991), *S. danae* 25 $m\,s^{-2}$, and for damselflies *C. splendens* 13 $m\,s^{-2}$ (Rüppell, 1989). The maximum non-dimensional thrust $\hat{T}$ generated by *S. sanguineum* was greater than that for *C. splendens*: 2.65 and 1.59, respectively. Again,

Table 5. *Probabilities that various kinematic parameters change with inclination of velocity ξ_V, inclination of thrust ξ_T, velocity* V *and thrust* T

		ξ_V		ξ_T	
Sympetrum sanguineum	$\bar{\chi}$	0.022		0.877	
		Forewings	Hindwings	Forewings	Hindwings
	β	0.013	0.001	0.520	0.654
		V		*T*	
	Φ	0.112	0.149	0.398	0.068
	ϕ_{max}	0.151	0.219	0.826	0.162
	$\bar{\phi}$	0.476	0.514	0.241	0.537
	ϕ_{min}	0.606	0.448	0.055	0.278
	n	0.424	0.347	0.558	0.426
		ξ_V		ξ_T	
Calopteryx splendens	$\bar{\chi}$	0.070		0.861	
		Forewings	Hindwings	Forewings	Hindwings
	β	0.119	0.037	0.014	0.065
		V		*T*	
	Φ	0.186	0.064	0.382	0.487
	ϕ_{max}	0.209	0.274	0.819	0.396
	$\bar{\phi}$	0.578	0.886	0.287	0.496
	ϕ_{min}	0.273	0.551	0.299	0.874
	n	0.840	0.728	0.077	0.076

All variables are defined in the text.

these values are similar to those already published for insects during take-off (Marden, 1987) with the equivalent values for $\hat{T}$ being 3.0 for a 125 mg *Sympetrum* dragonfly and 2.2 for a 149 mg *Mecistogaster* damselfly.

Although the dragonfly may typically fly faster and with greater acceleration than the damselfly, the non-dimensional velocities and accelerations were greater for *C. splendens*. The damselfly flew relatively further per wingbeat and accelerated relatively more per wingbeat than did the dragonfly. The main reason for this difference is that the damselfly flew at similar velocities but at wingbeat frequencies of half those of the dragonfly. Nevertheless, these two species are of similar mass, wing area and thus wing loading, and so the difference in the effectiveness of the wingstrokes must be due to the different wing kinematics. The stroke amplitude Φ was smaller and the wingbeat frequency *n* was greater for the dragonfly than for the damselfly, and it also had higher mean flapping velocities. Perhaps more importantly, the damselfly performed some degree of clap and fling, and beat its wings more synchronously, whereas the dragonfly wings did not touch at the top of the stroke and the forewings lagged by approximately 90 °.

The wing motions recorded here match some of those predicted from the morphology of the odonatan wing joint (Pfau, 1986, 1991). Pfau describes how the mechanism of odonatan wing motion is fundamentally different from that for the other Pterygota. In the Odonata, there is no tergal-arching mechanism for the downstroke, which is powered instead by the direct action of the basalar and subalar muscles; by contrast, the dorsolongitudinal muscle in other pterygotes causes the tergal plate to arch, which in turn leads to a depression of the wings. Because the wing motion is uncoupled from tergal arching, the Odonata are able to move all their wings relatively independently. The dorsolongitudinal muscle takes a different role in the Odonata; by tilting the tergal plate and thus the wing hinge, it allows the stroke plane to be altered relative to the body axis. The Anisoptera show further evolutionary modifications to the ancient flight mechanics of the Zygoptera/Anisozygoptera; they have almost completely reduced the dorsolongitudinal muscles in the metathorax and have completely reduced the pleuro-alary (stroke plane) muscles in both thoracic segments. The Anisoptera have thus simplified the motor system, and a steeper plane of wing movement has been achieved in both segments by developing a more vertical alignment of these segments.

Pfau (1986, 1991) suggests that the wing motion of the Anisoptera should have fewer degrees of freedom than that of the Zygoptera, with the anisopteran stroke plane at a relatively fixed orientation to the body. Differences in the wing joints also suggest that the Anisoptera must beat their hindwings through a smaller amplitude than their forewings. The kinematics reconstructed from the present study show that the dragonfly indeed has fewer degrees of freedom in its wing motion. In *S. sanguineum*, the stroke plane is almost rigidly fixed at inclinations of 48 ° and 50 ° from the longitudinal body axis for the fore- and hindwings, respectively. *C. splendens*, in

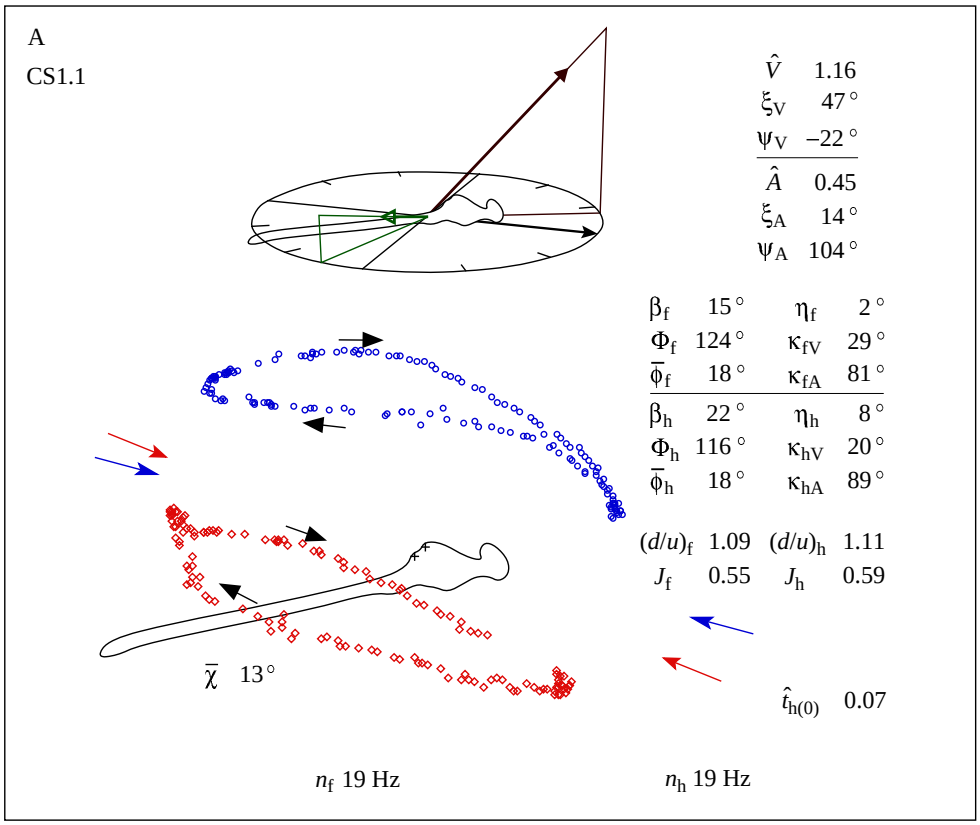

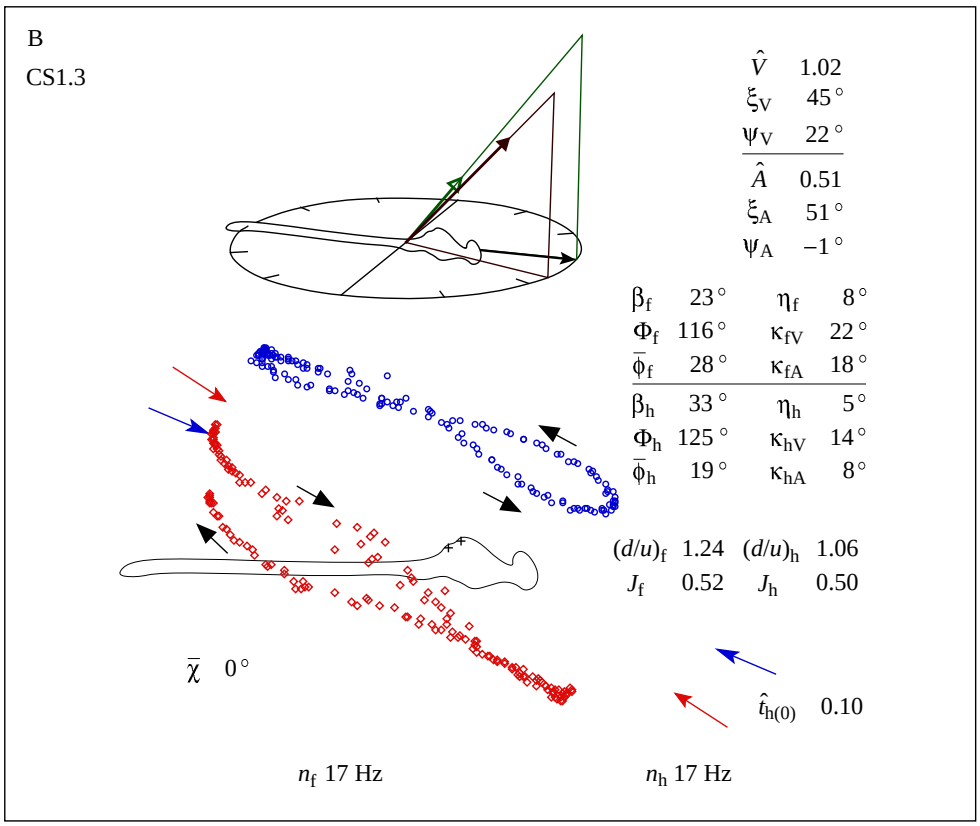

Fig. 8A,B. For legend see p. 578.

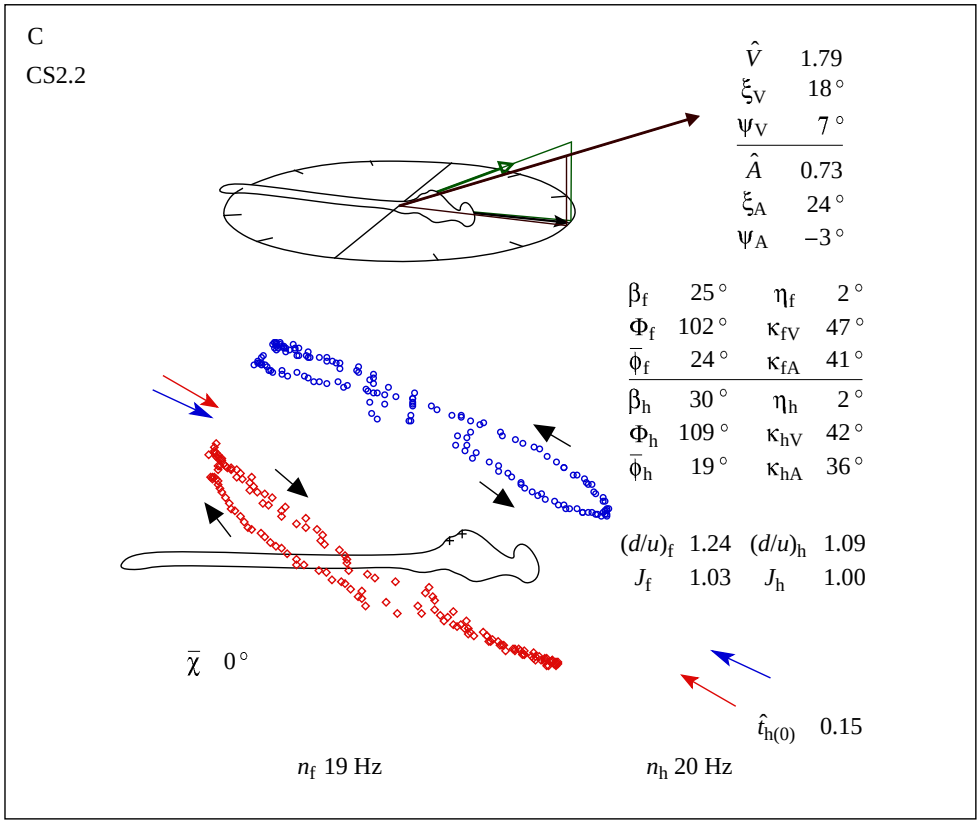

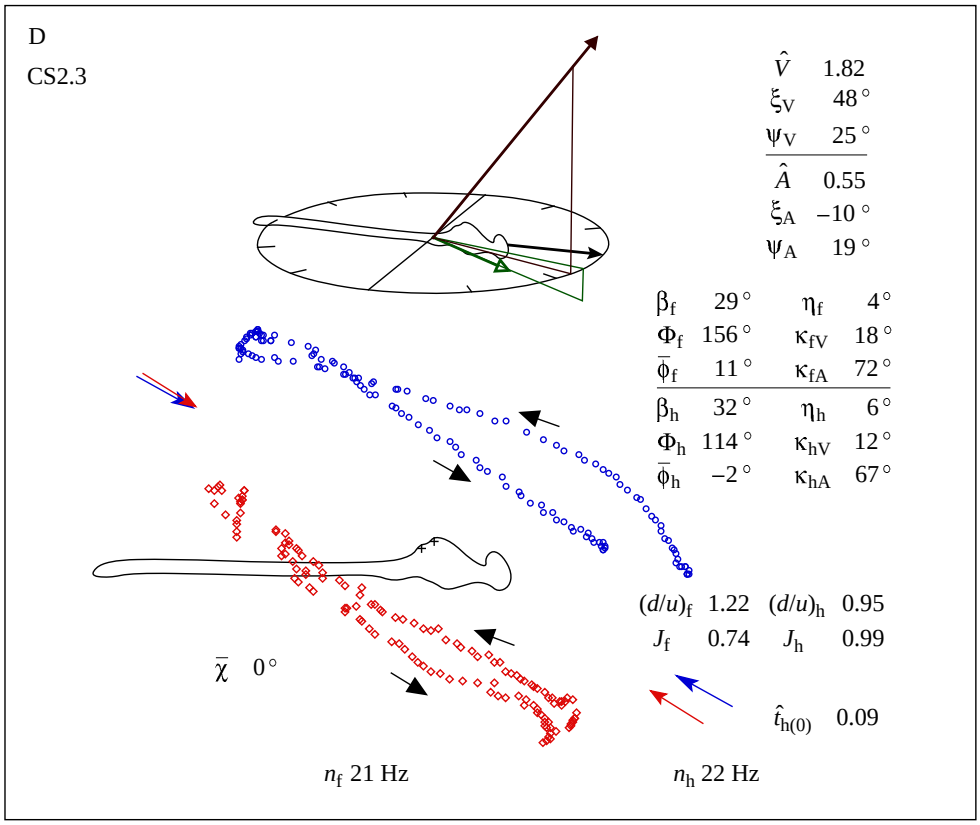

Fig. 8C,D. For legend see p. 578.

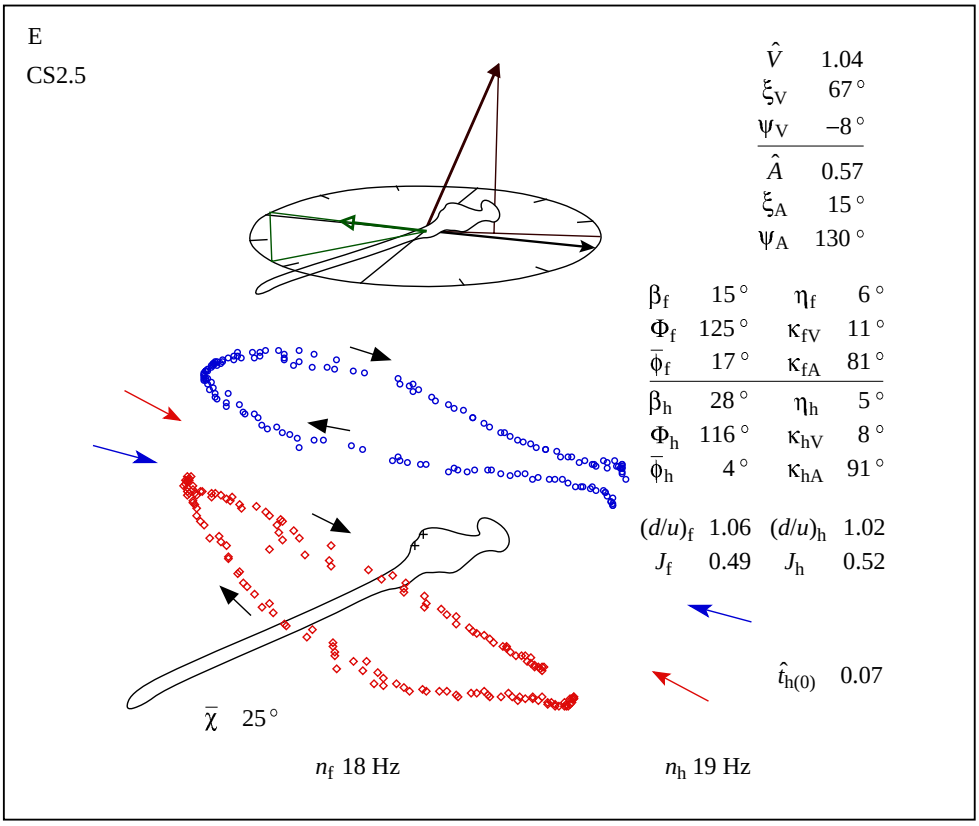

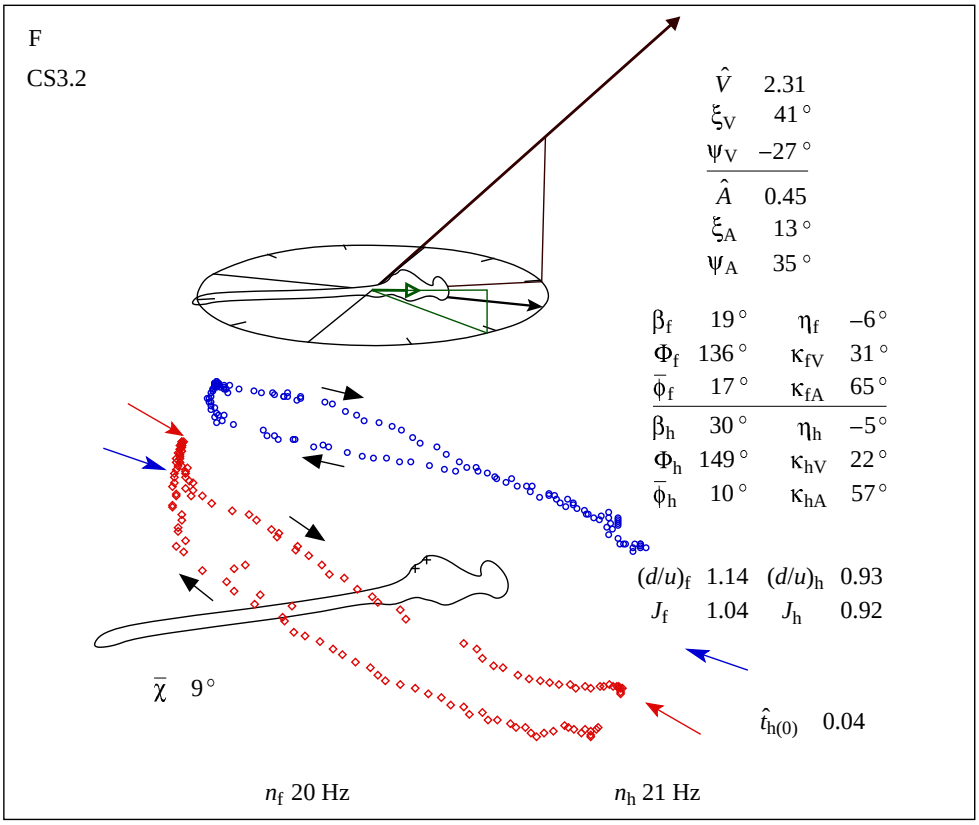

Fig. 8E,F. For legend see p. 578.

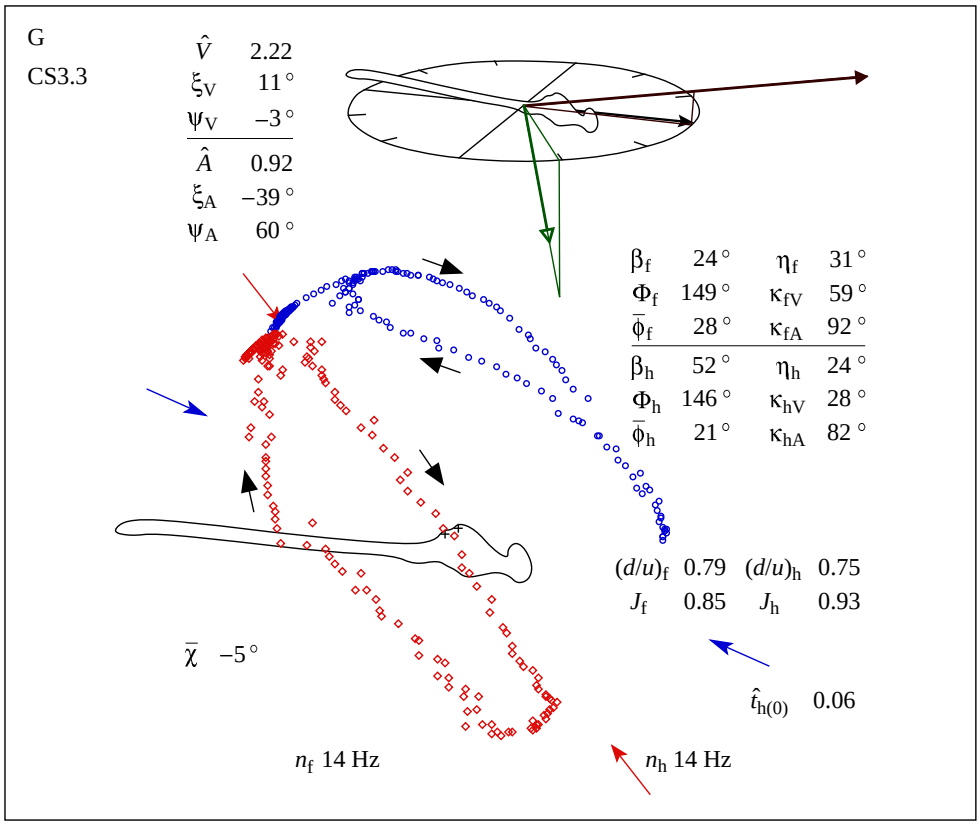

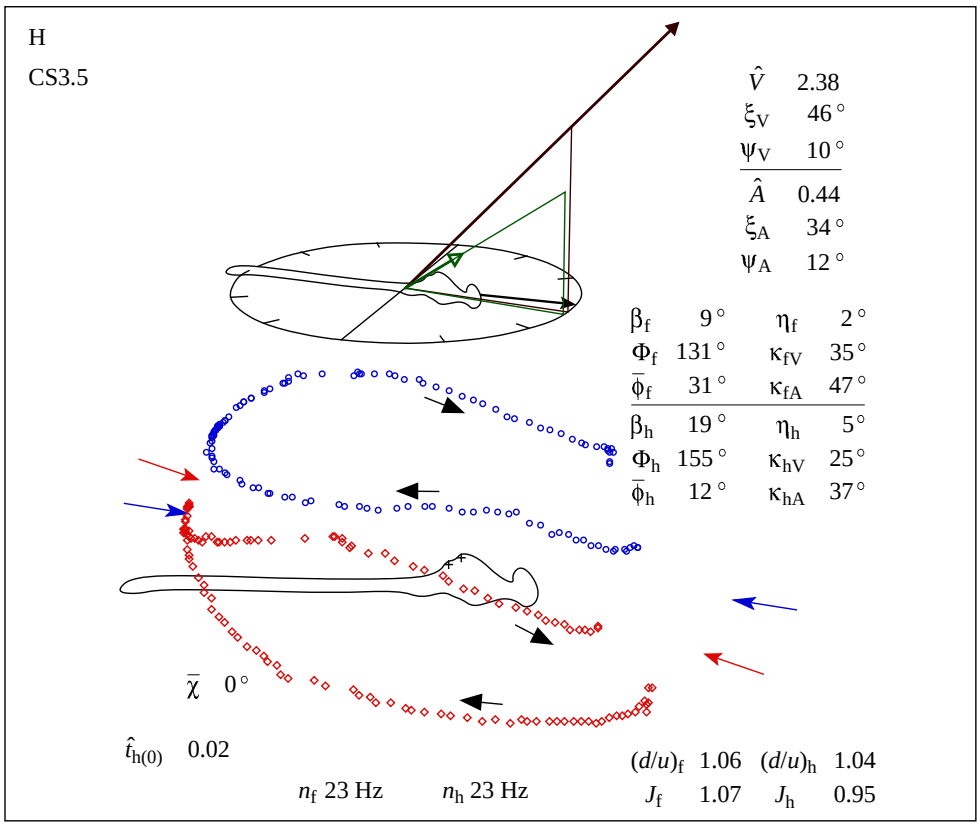

Fig. 8G,H. For legend see p. 578.

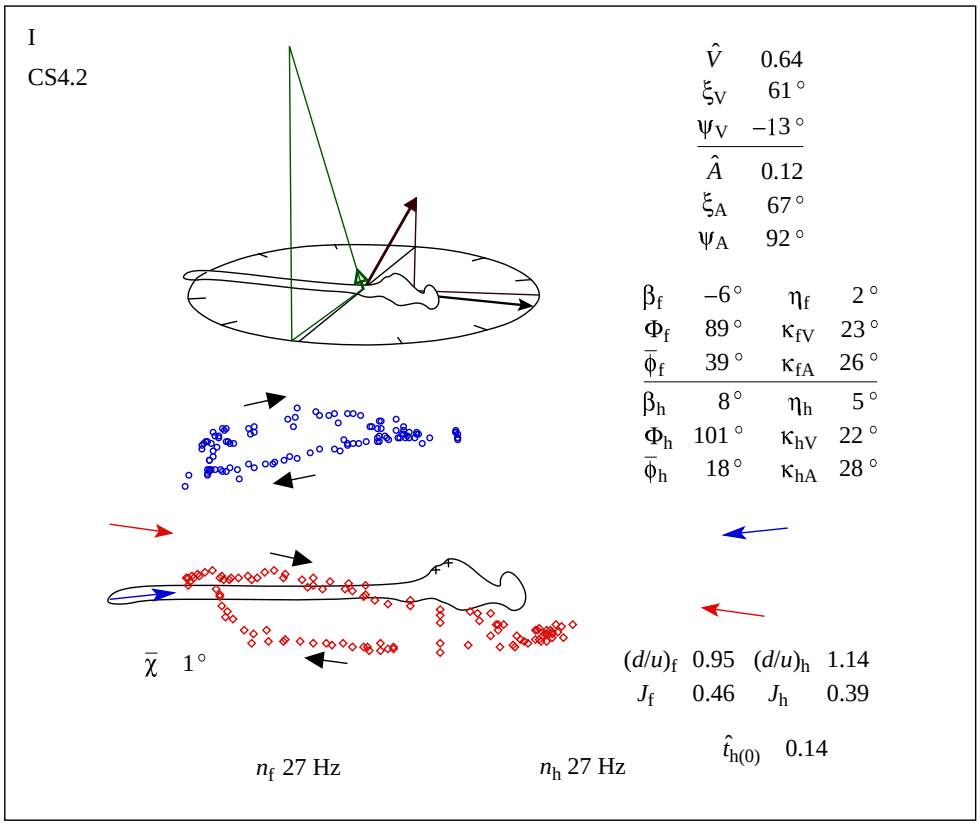

Fig. 8. (A–I) The analysed wingbeats for *Calopteryx splendens*, showing the vectors for non-dimensional velocity and non-dimensional acceleration (upper drawings), and the reconstructed wingtip path (lower drawings). Full details of these diagrams along with definitions of the parameters can be found in the text.

contrast, varies its stroke plane from −5 ° to 53 ° relative to the body axis. Also, within each wingstroke, *C. splendens* had a greater freedom of wing motion from the stroke plane, as shown by a greater variation in θ; the wing motion of *S. sanguineum* was much more confined to the stroke plane. The hindwings of *S. sanguineum* actually beat through greater stroke amplitudes than did the forewings, which is in contrast to Pfau's (1986, 1991) predictions.

Stroke plane angles and mean body angles

The orientation of the dragonfly during flight will be a compromise between the orientation of the stroke plane and that of the body, and this has been shown for Anisoptera in general (Rüppell and Hilfert, 1993). The wings are more effective at producing thrust when the stroke plane is normal to the direction of that thrust (Wakeling and Ellington, 1997*b*). The body experiences least drag D_{par} when it is aligned to face the direction of the relative velocity, as D_{par} is minimised at small body angles (Wakeling and Ellington, 1997*a*). Indeed, during the horizontal forward flight of insects in general, body angles decrease with increasing velocity to minimise the cost of D_{par}. Correlations have been found between the body angle and flight velocity for the dragonfly *Anax parthenope* (Azuma and Watanabe, 1988), *Drosophila* spp. (Vogel, 1966; Götz, 1968; David, 1979), the honeybee (Esch *et al.* 1975), the bumblebee *Bombus terrestris* (Dudley and Ellington, 1990; Cooper, 1993) and neotropical butterflies (Dudley, 1990). For the damselfly, where the alignment of the stroke plane is relatively independent of the body direction, it might be expected that the stroke plane can be normal to the direction of the thrust at the same time as the body faces the relative velocity. The dragonfly, in contrast, has a more restricted wing motion relative to the body; its orientation may be more of a compromise.

The mean body angle for *S. sanguineum* increases as the inclination of the flight velocity increases, suggesting that it is maintaining a low D_{par} orientation. There are no significant regressions between the mean body angle and the stroke plane angle with the direction of thrust. The angles between the normals to the stroke planes and the direction of the velocity, κ_V, are smaller than the angles to the direction of the thrust κ_T, and there is less variance in κ_V than in κ_T. The orientation which *S. sanguineum* adopted during these sequences seems to have been dominated more by aligning the body towards the relative flight direction and thus minimising D_{par} than by positioning the stroke planes to face the thrust. It should be noted that the flights recorded here were all at a reasonable forward velocity $\hat{V}$>0.65, but at low flight speeds the parasite drag will be a negligible concern. If the mean values of κ_T of approximately 19 ° are considered typical for *S. sanguineum*, then there is little evidence to suggest that it would hover with steeply inclined stroke planes, as suggested for Odonata in general (Weis-Fogh, 1973) and *Aeshna juncea* in particular (Norberg, 1975).

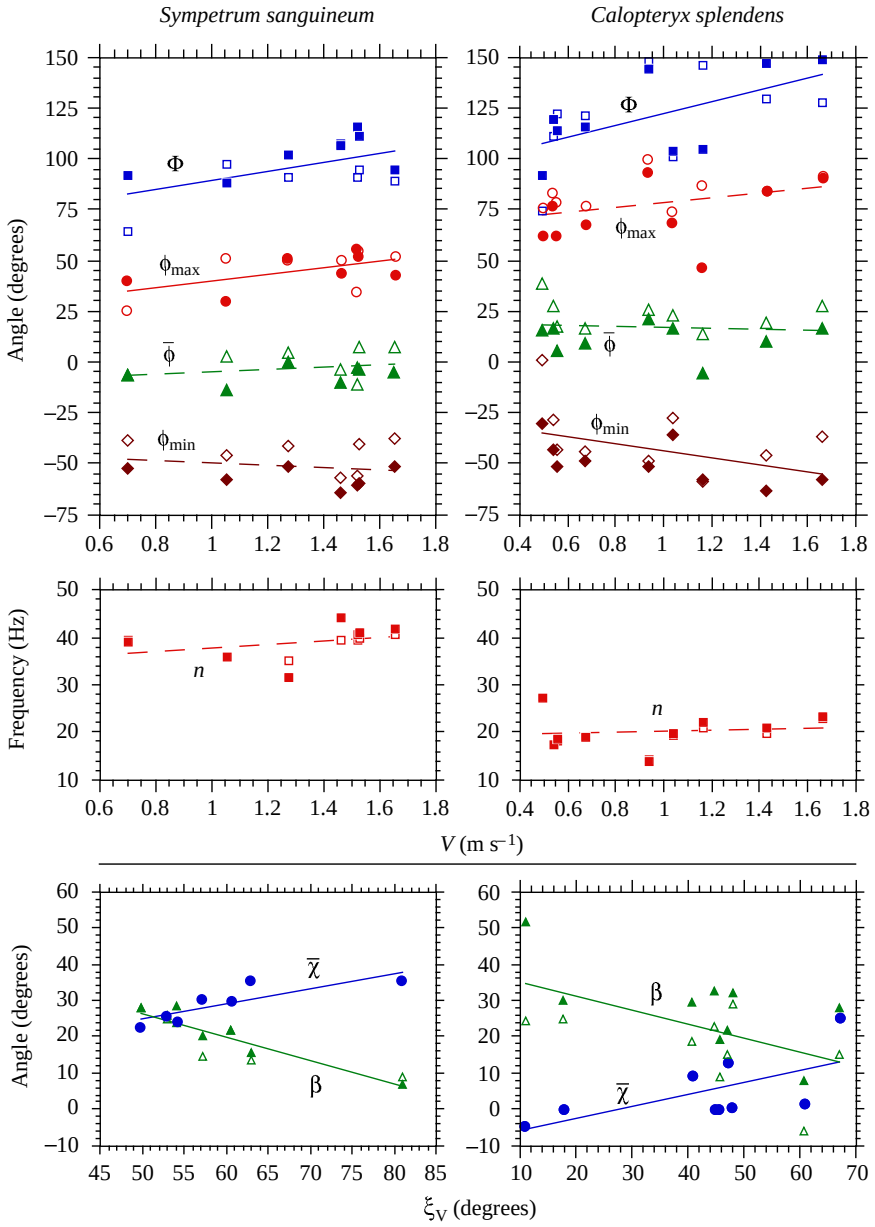

Fig. 9. Changes in various stroke parameters with velocity V and inclination of velocity ζ_V. Open symbols represent data for the forewings, whilst filled symbols represent data for the hindwings. Regression lines are drawn for the pooled data from both the fore- and hindwings; these lines are solid where $P<0.1$ and dashed where $P>0.1$. Parameters are defined in the text.

C. splendens adopted a mixed strategy for its body orientation during these flight sequences. During half the sequences, the body was nearly horizontal despite its inclined velocity direction, and for the other half it showed an increasing body angle with increasing flight inclination. The flights with horizontal bodies were not exclusively those at the lowest velocities, where D_{par} would be smallest. The stroke planes faced the direction of the thrust more closely than the direction of the velocity, with the means and variances of κ_T for the forewings being smaller than those of κ_V. This highlights the extra freedom that the damselfly has in its wing motion: it can align its body to the flight direction at the same time that its stroke planes are facing the thrust. In cases where the thrust is rapidly changing, the damselfly does not necessarily need to realign its body in order to face its stroke planes in the new thrust direction. Evidence from the present study suggests that *C. splendens* would hover with horizontal stroke planes in a manner categorised as 'normal hovering' (Weis-Fogh, 1972, 1973; Ellington, 1984*a*).

Wingstroke amplitudes and wingbeat frequency

Increases in the stroke amplitude Φ will increase the relative velocity of the wing and hence the forces produced during a wingstroke. However, there have been few clear correlations of Φ with flight velocity in insects. The dragonfly *Anax parthenope* (Azuma and Watanabe, 1988) showed no correlation of Φ with velocity. Sotavalta (1947) suggested that the amplitude for the sphingid *Sphinx ligustri* may be higher during slow forward flight than during hovering, but Cooper (1993) reported a general decrease in Φ with velocity for the bumblebee *Bombus terrestris*. Magnan (1934) noted a general decrease in Φ for free-flying insects with increased velocity. Studies on tethered flight

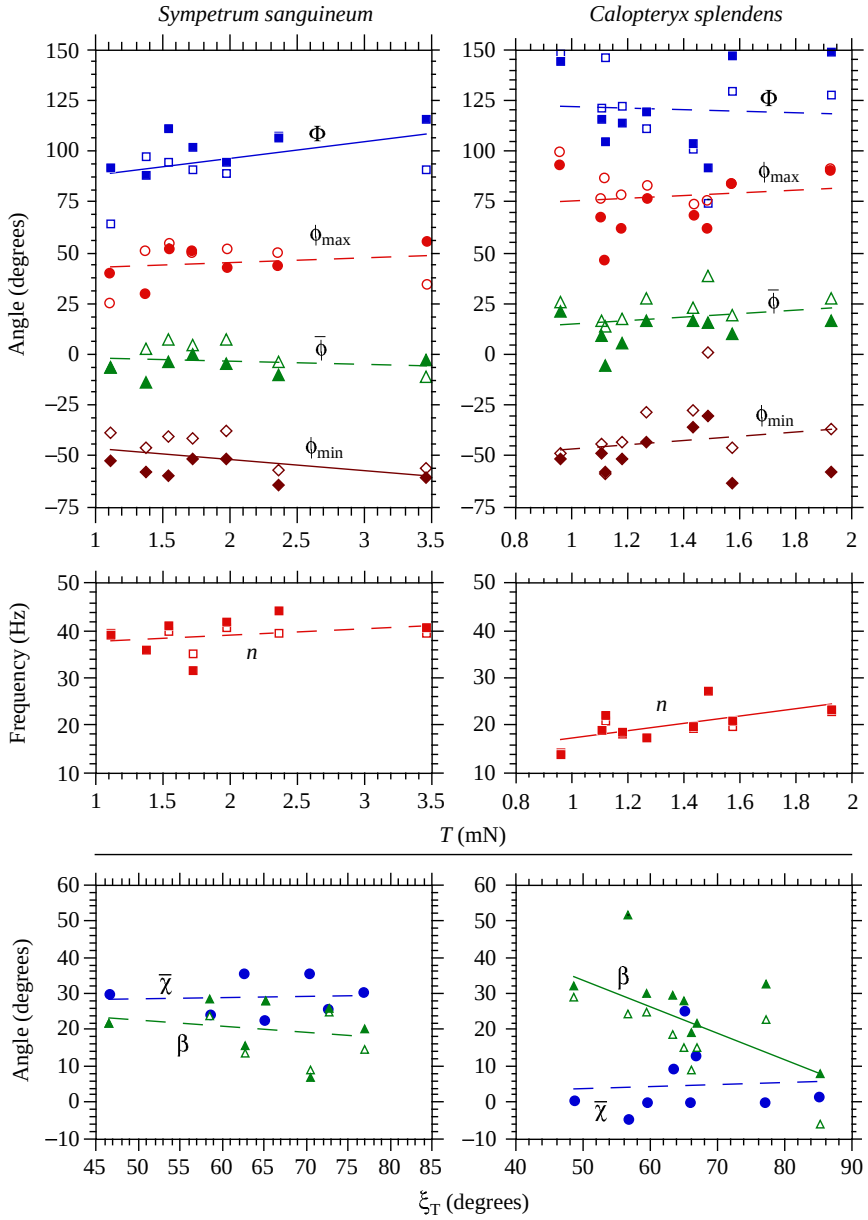

Fig. 10. Changes in various stroke parameters with thrust T and inclination of thrust ζ_T. Open symbols represent data for the forewings, whilst filled symbols represent data for the hindwings. Regression lines are drawn for the pooled data from both the fore- and hindwings; these lines are solid where $P<0.1$ and dashed where $P>0.1$. Parameters are defined in the text.

have consistently shown a decrease in Φ with velocity for tethered *Calliphora erythrocephala*, *Locusta migratoria*, the dragonfly *Orthetrum cancellatum* (Gewecke, 1967, 1970, 1974, respectively) and the fly *Muscina stabulans* (Hollick, 1940). It is debatable whether such tethered results are applicable to free flight (Rüppell, 1989), especially when the insects are in fixed tethers and are unable to regulate their body angles. The tethered flight of locusts (Baker *et al.* 1981) and Heteroptera (Betts, 1986) is known to differ from that in the field.

In the present study, there were no significant regressions between any of the positional parameters and velocity (Table 5). However, some trends were apparent and can be seen more easily in Figs 9 and 10. There is a slight increase in Φ with velocity for both *S. sanguineum* and *C. splendens*. In general, these increases in Φ are generated by both increases in ϕ_{max} and decreases in ϕ_{min}, with the mean positional angle of the wing $\bar{\phi}$ remaining reasonably invariant. The only significant regression between the positional parameters and thrust was for ϕ_{max} for the damselfly, and only when flight CS3.3 was ignored. This regression does show how the proximity of the hindwings during a partial fling affects the forces produced during that fling.

Increases in the wingbeat frequency n will also increase the relative velocity of the wing and hence the forces produced during a wingstroke. Different trends of n with velocity have been shown for different insects. In the dragonfly *Anax parthenope*, no correlation was found (Azuma and Watanabe, 1988), and wingbeat frequency was observed to be remarkably constant for *C. splendens* under 'all experimental conditions' (Rudolph, 1976*b*). Lack of correlation between n and velocity has also been reported for *Drosophila virilis* (Vogel, 1967) and bumblebees (Dudley and Ellington, 1990; Cooper, 1993).

Positive correlations, however, have been found between *n* and velocity for the locust both while free-flying (Baker *et al.* 1981) and tethered (Gewecke, 1975). The wingbeat frequency of dragonflies during free flight has been shown to be correlated with body temperature (Sotavalta, 1954; May, 1981).

In the present study, there were no significant regressions between *n* and either velocity or thrust (Table 5) except that the wingbeat frequency of *C. splendens* increases with thrust (Fig. 10).

Wing interactions; phasing relationships and clap and fling

The damselflies flew with higher non-dimensional velocities and accelerations than the dragonflies, showing that they were moving relatively further and accelerating relatively more per wingbeat. The mean non-dimensional damselfly thrusts were 82 % of the dragonfly values despite flying at half the wingbeat frequency. The damselfly wingbeat must therefore be more effective at producing aerodynamic force than the dragonfly wingbeat.

The main differences between the wingbeat kinematics of *C. splendens* and *S. sanguineum* are that the damselfly performs clap and flings or partial flings, its fore- and hindwings beat almost exactly in phase, and its wingbeat frequency is half that of the dragonfly. *S. sanguineum* wings, in contrast, do not come close together at the top of their stroke and they beat with the forewings lagging by approximately 90 °. The precise interactions between the fore- and hindwing pairs of the dragonfly are not fully understood, but the present study shows (see also Alexander, 1984, 1986; Lan, 1979; Rüppell, 1989) that wingbeats producing the greatest thrusts are those where the fore- and hindwings beat almost synchronously.

Some of Rüppell's films show Calopterygidae manoeuvres in which the damselfly rapidly accelerates backwards while using a synchronous fore- and hindwing downstroke. Such a wingstroke will effectively squeeze air out from between the wings, and a large aerodynamic force is produced by the profile drag; this is discussed in more detail by Wakeling and Ellington (1997*b*). The geometry of the wing motion from the flights in the present study, however, would not lead to useful force production by profile drag (Wakeling and Ellington, 1997*b*). The clap and fling is a recognised mechanism for lift enhancement and is employed by the damselfly but not the dragonfly; this is probably the main cause for the greater thrust produced by the damselfly wingbeat.

Aerodynamic mechanisms of dragonfly flight

The flights described in this study covered a threefold range of thrust for *S. sanguineum* and a twofold range for *C. splendens*. If the aerodynamic force were to be produced by entirely quasi-steady mechanisms, then it should be expected that there would be a correlation between thrust and the kinematic factors governing force production, i.e. stroke amplitude, wingbeat frequency and angle of attack. The angle of attack was not measured in this study; however, the lift-to-drag polars for these two species demonstrate little change in lift coefficient over a wide range of angles (Wakeling and Ellington, 1997*a*), showing that there would be little effect on the quasi-steady lift of changes in angle of attack. Additionally, Azuma and Watanabe (1988) failed to find any trend in angle of attack over a fourfold range of velocity for *Anax parthenope*. The lack of correlation between any of these kinematic parameters and thrust suggests that aerodynamic force must be produced by mechanisms that are not entirely quasi-steady in nature. Wing flex during supination and pronation was not quantified in this study, but it may be a possible method for additional force generation during the stroke. The present study thus adds to the growing body of evidence that unsteady lift-producing mechanisms must be involved during insect flight. The aerodynamics of the flights from this study are considered in further detail in Wakeling and Ellington (1997*b*).

References

ALEXANDER, D. E. (1984). Unusual phase relationships between the forewings and hindwings in flying dragonflies. *J. exp. Biol.* **109**, 379–383.

ALEXANDER, D. E. (1986). Wind tunnel studies of turns by flying dragonflies. *J. exp. Biol.* **122**, 81–98.

AZUMA, A. (1992). *The Biokinetics of Flying and Swimming.* pp. 138–148. Berlin: Springer-Verlag.

AZUMA, A., AZUMA, S., WATANABE, I. AND FURUTA, T. (1985). Flight mechanics of a dragonfly. *J. exp. Biol.* **116**, 79–107.

AZUMA, A. AND WATANABE, T. (1988). Flight performance of a dragonfly. *J. exp. Biol.* **137**, 221–252.

BAKER, P. S., GEWECKE, M. AND COOTER, R. J. (1981). The natural flight of the migratory locust, *Locusta migratoria.* III. Wingbeat frequency, flight speed and attitude. *J. comp. Physiol.* **141**, 233–237.

BENNETT, L. (1977). Clap and fling aerodynamics – an experimental evaluation. *J. exp. Biol.* **69**, 261–272.

BETTS, C. R. (1986). The kinematics of Heteroptera in free flight. *J. Zool., Lond. B* **1**, 303–315.

CHADWICK, L. E. (1940). The wing motion of the dragonfly. *Bull. Brooklyn ent. Soc.* **35**, 109–112.

COOPER, A. J. (1993). Limitations on bumblebee flight performance. PhD thesis. Cambridge University.

COOTER, R. J. AND BAKER, P. S. (1977). Weis-Fogh clap and fling mechanism in *Locusta*. *Nature* **269**, 53–54.

DAVID, C. T. (1979). Optomotor control of speed and height by free-flying *Drosophila*. *J. exp. Biol.* **82**, 389–392.

DICKINSON, M. H. (1994). The effects of wing rotation on unsteady aerodynamic performance at low Reynolds numbers. *J. exp. Biol.* **192**, 179–206.

DUDLEY, R. (1990). Biomechanics of flight in neotropical butterflies: morphometrics and kinematics. *J. exp. Biol.* **150**, 37–53.

DUDLEY, R. AND ELLINGTON, C. P. (1990). Mechanics of forward flight in bumblebees. I. Kinematics and morphology. *J. exp. Biol.* **148**, 19–52.

EDWARDS, R. H. AND CHENG, H. K. (1982). The separation vortex in the Weis-Fogh circulation-generation mechanism. *J. Fluid Mech.* **120**, 463–473.

ELLINGTON, C. P. (1984*a*). The aerodynamics of hovering insect flight. I. The quasi-steady analysis. *Phil. Trans. R. Soc. Lond. B* **305**, 1–15.

ELLINGTON, C. P. (1984*b*). The aerodynamics of hovering insect flight. III. Kinematics. *Phil. Trans. R. Soc. Lond. B* **305**, 41–78.

ELLINGTON, C. P. (1984*c*). The aerodynamics of hovering insect flight. IV. Aerodynamic mechanisms. *Phil. Trans. R. Soc. Lond. B* **305**, 79–113.

ENNOS, A. R. (1988). The importance of torsion in the design of insect wings. *J. exp. Biol.* **140**, 137–160.

ENNOS, A. R. (1989). The kinematics and aerodynamics of the free flight of some Diptera. *J. exp. Biol.* **142**, 49–85.

ESCH, H., NACHTIGALL, W. AND KOGGE, S. N. (1975). Correlations between aerodynamic output, electrical activity in the indirect flight muscles and wing positions of bees flying in a servomechanically controlled wind tunnel. *J. comp. Physiol.* **100**, 147–159.

GEWECKE, M. (1967). Die Wirkung von Luftstroung auf die Antennen und das Flugverhalten der blauen Schmeissfliege (*Calliphora erythrocephala*). *Z. vergl. Physiol.* **54**, 121–164.

GEWECKE, M. (1970). Antennae: another wind-sensitive receptor in locusts. *Nature* **225**, 1263–1264.

GEWECKE, M. (1974). Role of antennae of the dragonfly *Orthetrum cancellatum* in flight control. *Nature* **249**, 584–585.

GEWECKE, M. (1975). The influence of the air current sense organs on the flight behaviour of *Locusta migratoria*. *J. comp. Physiol.* **103**, 79–95.

GÖTZ, K. G. (1968). Flight control in *Drosophila* by visual control of motion. *Kybernetik* **4**, 199–208.

GRABOW, K. AND RÜPPELL, G. (1995). Wing loading in relation to body size and flight characteristics of European Odonata. *Odonatologica* **24**, 175–186.

HANKIN, E. H. (1921). The soaring flight of dragonflies. *Proc. Camb. phil. Soc.* **20**, 460–465.

HAUSSLING, H. J. (1979). Boundary-fitted coordinates for accurate numerical solution of multi-body flow problems. *J. comput. Phys.* **30**, 511–552.

HOLLICK, F. S. J. (1940). On the flight of the dipterous fly *Muscina stabulans* Fallen. *Phil. Trans. R. Soc. Lond. B* **230**, 357–390.

LAN, C. E. (1979). The unsteady quasi-vortex-lattice method with applications to animal propulsion. *J. Fluid Mech.* **93**, 747–765.

LIGHTHILL, M. J. (1973). On the Weis-Fogh mechanism of lift generation. *J. Fluid Mech.* **60**, 1–17.

LUTTGES, M. W. (1989). Accomplished insect fliers. In *Frontiers in Experimental Fluid Mechanics. Lecture Notes in Engineering 46* (ed. M. Gad-el-Hak), pp. 429–456. Berlin: Springer-Verlag.

MAGNAN, A. (1934). *La Locomotion chez les Animaux*. I. *Le Vol des Insectes*. Paris: Hermann et Cie.

MARDEN, J. H. (1987). Maximum lift production during takeoff in flying animals. *J. exp. Biol.* **130**, 235–258.

MAXWORTHY, T. (1979). Experiments on the Weis-Fogh mechanism of lift generation by insects in hovering flight. Part 1. Dynamics of the 'fling'. *J. Fluid Mech.* **93**, 47–63.

MAY, M. L. (1981). Wingstroke frequency of dragonflies (Odonata: Anisoptera) in relation of temperature and body size. *J. comp. Physiol.* **144**, 229–240.

MAY, M. L. (1991). Dragonfly flight: power requirements at high speed and acceleration. *J. exp. Biol.* **158**, 325–342.

NEWMAN, D. J. S. (1982). The functional wing morphology of some Odonata. PhD thesis. Exeter University.

NORBERG, R. Å. (1975). Hovering flight of the dragonfly *Aeschna juncea* L., kinematics and aerodynamics. In *Swimming and Flying in Nature*, vol. 2 (ed. T. Y. Wu, C. J. Brokaw and C. Brennen), pp. 763–781. New York: Plenum Press.

PFAU, H. K. (1986). Untersuchungen zur Konstruktion, Funktion und Evolution des Flugapparates der Libellen. *Tijdschr. Ent.* **129**, 35–123.

PFAU, H. K. (1991). Contributions of functional morphology to the phylogenetic systematics of Odonata. *Ad. Odonatol.* **5**, 109–141.

RUDOLPH, R. (1976*a*). Preflight behaviour and the initiation of flight in *Calopteryx splendens* (Harris) (Zygoptera: Calopterygidae). *Odonatologica* **5**, 59–64.

RUDOLPH, R. (1976*b*). Some aspects of wing kinematics in *Calopteryx splendens* (Harris) (Zygoptera: Calopterygidae). *Odonatologica* **5**, 119–127.

RÜPPELL, G. (1985). Kinematic and behavioural aspects of the flight of the male Banded Agrion *Calopteryx splendens* L. In *Insect Locomotion* (ed. M. Gewecke and G. Wendler), pp. 195–204. Berlin, Hamburg: Parey.

RÜPPELL, G. (1989). Kinematic analysis of symmetrical flight manoeuvres of Odonata. *J. exp. Biol.* **144**, 13–42.

RÜPPELL, G. AND HILFERT, D. (1993). The flight of the relict dragonfly *Epiophlebia superstes* in comparison with that of the modern Odonata (Anisozygoptera: Epiophlebiidae). *Odonatologica* **22**, 295–309.

SAHARON, D. AND LUTTGES, M. W. (1988). Visualisation of unsteady separated flow produced by mechanically driven dragonfly wing kinematics model. *AIAA Paper* no. 88-0569.

SOMPS, C. AND LUTTGES, M. W. (1985). Dragonfly flight: novel uses of unsteady separated flows. *Science* **228**, 1326–1329.

SOTAVALTA, O. (1947). The flight-tone (wing-stroke frequency) of insects. *Acta ent. Fenn.* **4**, 1–117.

SOTAVALTA, O. (1954). The effect of wing inertia on the wing-stroke frequency of moths, dragonflies and cockroach. *Ann. ent. Fenn.* **20**, 93–101.

SPEDDING, G. R. AND MAXWORTHY, T. (1986). The generation of circulation and lift in a rigid two-dimensional fling. *J. Fluid Mech.* **165**, 247–272.

SUNADA, S., KAWACHI, K., WATANABE, I. AND AZUMA, A. (1993). Fundamental analysis of three-dimensional 'near-fling'. *J. exp. Biol.* **183**, 217–248.

VOGEL, S. (1966). Flight in *Drosophila* I. Flight performance of tethered flies. *J. exp. Biol.* **44**, 567–578.

VOGEL, S. (1967). Flight in *Drosophila* II. Variations in stroke parameters and wing contour. *J. exp. Biol.* **46**, 383–392.

WAKELING, J. M. (1997). Odonatan wing and body morphologies. *Odonatologica* **26**, 35–52.

WAKELING, J. M. AND ELLINGTON, C. P. (1997*a*). Dragonfly flight. I. Gliding flight and steady-state aerodynamics. *J. exp. Biol.* **200**, 543–556.

WAKELING, J. M. AND ELLINGTON, C. P. (1997*b*). Dragonfly flight. III. Lift and power requirements. *J. exp. Biol.* **200**, 583–600.

WEIS-FOGH, T. (1967). Respiration and trachael ventilation in locusts and other flying insects. *J. exp. Biol.* **47**, 561–587.

WEIS-FOGH, T. (1972). Energetics of hovering flight in hummingbirds and *Drosophila*. *J. exp. Biol.* **56**, 79–104.

WEIS-FOGH, T. (1973). Quick estimates of flight fitness in hovering animals, including novel mechanisms for lift production. *J. exp. Biol.* **59**, 169–230.

WOOTTON, R. J. (1991). The functional morphology of the wings of Odonata. *Adv. Odonatol.* **5**, 153–169.

WU, J. AND HU-CHEN, H. (1984). Unsteady aerodynamics of articulate lifting bodies. *AIAA Paper* no. 2184.

ZANKER, J. M. AND GÖTZ, K. G. (1990). The wing beat of *Drosophila melanogaster*. II. Dynamics. *Phil. Trans. R. Soc. Lond. B* **327**, 19–44.